C. 1.

THE TRANSVERSE DYNAMICS OF ROTATING IMPERFECT DISKS

by

GREGORY WILLIAM ROSVAL
B.A.Sc., University of British Columbia, 1976

A THESIS SUBMITTED IN PARTIAL FULFILLMENT OF
THE REQUIREMENTS FOR THE DEGREE OF

MASTER OF APPLIED SCIENCE

in

THE FACULTY OF GRADUATE STUDIES

(Department of Mechanical Engineering)

We accept this thesis as conforming
to the required standard.

THE UNIVERSITY OF BRITISH COLUMBIA

January 1981

In presenting this thesis in partial fulfillment of the requirements for an advanced degree at the University of British Columbia, I agree that the Library shall make it freely available for reference and study. I further agree that permission for extensive copying of this thesis for scholarly purposes may be granted by the Head of my Department or by his representatives. It is understood that copying or publication of this thesis for financial gain shall not be allowed without my written permission.

Department of Mechanical Engineering
The University of British Columbia
2075 Wesbrook Place
Vancouver, Canada
V6T 1W5
December 1, 1980

ABSTRACT

The transverse motions of circular saws have undesirable effects on many aspects of circular sawing. Due to current high manufacturing costs, substantial savings may be realized if these transverse motions can be reduced.

In this thesis a circular saw is modelled as a rotating imperfect disk acted upon by a transverse, non-oscillatory point load stationary in space. Such a model is known to accurately predict certain relevant aspects of the behaviour of a circular saw in its operating environment.

Initially the free response of a non-rotating perfect disk is considered. This model is then refined by considering the effects of rotational stresses and small imperfections within the disk. The response of such a disk to an oscillatory load is determined, from which the response to a non-oscillatory load may be determined as a special case of particular interest.

Experimental results are given which quantitatively confirm the theory presented.

ACKNOWLEDGEMENTS

I wish to thank Professors H. Vaughan and S. Hutton for their supervision of the thesis. I am also grateful to Dr. J. Brdicko of Canadian Car Limited both for his advice and for the loan of some of the experimental equipment that was used. Mr. P. Hurren and Mr. J. Richards of the University of British Columbia were very helpful in assisting me in the development of a functioning experimental set-up.

The fine job of typing this thesis was done by Mrs. Lynn Main, whom I wish to thank. Finally, I would like to acknowledge the patience and encouragement offered by my wife Sandy during the preparation of this thesis.

TABLE OF CONTENTS

NOTATION

a	clamp radius
b	disk radius
D	flexural rigidity; energy dissipated by damping
E	Young's Modulus
f_n	observed frequency
g_n	damping dissipation coefficient
h	disk half-thickness
M_n	generalized force
P	amplitude of load
p_n	natural frequency
q_n	natural frequency
R_n	radial displacement function
r	radial coordinate
r_p	radial location of load
T	temporal response function; kinetic energy
t	time coordinate
U	strain energy
u	displacement in space-fixed coordinates
V_n	proportionality constant for membrane frequency
w	displacement in disk-fixed coordinates
α_n, β_n	angular phase angles
β_n	strain energy coefficient
ε_n, t_o	temporal phase angles
γ	angular space-fixed coordinate

λ	non-dimensional frequency parameter
Θ	angular displacement function
θ	angular disk-fixed coordinate
θ_p	angular location of load in the disk coordinate system
μ	kinetic energy coefficient
$\sigma\ (r)$	radial membrane stress
$\sigma\ (\theta)$	tangential membrane (hoop) stress
ρ	mass density
ν	Poisson's ratio
Ω	disk rotational speed
ω	excitation frequency
τ	variable coefficient in radial function
ξ	damping ratio

LIST OF FIGURES

I. Introduction

The use of circular saws in the manufacture of lumber is very common, and in an attempt to reduce the costs associated with this process much research has been conducted. Many of the problems resulting from the use of a circular saw may be attributed to motions of the saw in the direction normal to its plane. These motions, which are referred to as transverse vibrations, have an undesirable effect on cutting accuracy, kerf losses, the quality of the cut surfaces, saw life and ambient noise levels. One of the primary goals of researchers in this area is to reduce the kerf losses by making the saw thinner. This must be done without suffering the adverse effects caused by an increase in the transverse vibrations resulting from a reduction in the lateral stiffness of the saw.

In attempting to predict the behaviour of a circular saw in its working environment, many difficulties are encountered. Since the saw and its environment are continually changing, no complete solution exists which considers all aspects of the problem simultaneously. However, it is possible to model this system in a way such that useful qualitative and quantitative results may be determined from fundamental principles.

Most simply, a circular saw may be modelled as a non-rotating, unclamped complete disk. The natural frequencies and shapes of the free vibrations of such a disk were determined by Kirchoff in 1850[1]. Later in that century Rayleigh made a significant contribution to this problem, in particular in reconciling theoretical predictions with experimental results[2]. He introduced the idea that small imperfections within the disk could significantly affect its behaviour. Near the end of the 19th century Zenneck formalized the ideas of Rayleigh regarding the influence of imperfections on the free vibrations of a disk[3].

The inclusion of stresses due to the rotation of the disk was the next major step in the development of the model. This was done by Lamb and Southwell in 1921[4]. It was in this work that Southwell's Theorem was first introduced. This theorem states that under certain conditions an approximate method is available which establishes a lower bound on the fundamental frequency of vibration of a body. This work, however, did not consider the influence of a central clamp covering a portion of the disk. Later that year Southwell published a paper in which the effects of a clamp were considered, and where his theorem was demonstrated with numerical examples[5].

It wasn't until 1957 that the experimentally observed forced response of a rotating disk was satisfactorily explained. This information was made available in a paper by Tobias and Arnold, where it was shown that achieving agreement between theoretical and experimental results requires considering the effects of minor imperfections within the disk[6].

The directions of research since this time have generally fallen into one or more of the following catagories; the control of membrane stresses[7,8,9,10,11,12] altering saw geometries[13,14] and external control methods.[15,16] Although numerical results can be obtained when the problem can be mathematically modelled, obtaining a suitable model which includes all aspects of the problem presents a major difficulty. For this reason an approach combining both theory and experimentation is very useful.

Because experimentation should be an important part of an investigation in this field, this thesis deals with rotating disks on both a theoretical and an experimental basis. It is the purpose of this thesis to present a theory of the forced response of rotating disks and to present experimental results which verify this theory. While a detailed theoretical development of the forced response of idealized disks is given, emphasis is placed on the theory required to account for the departure of the characteristics of real disks from those of idealized disks.

II The Theory of Rotating Disks

Two types of disks are analyzed in this thesis. The first are what are referred to as "perfect disks". These disks are homogeneous, isotropic, completely circular and are of constant thickness throughout. The second type, called "imperfect disks", possess material properties and geometries which depart slightly from those of perfect disks. All real disks are to some extent imperfect, and the influences of these imperfections on the disks' behaviour must be taken into account when experimental results are interperted.

Because the disk is rotating in space while observations are made from points stationary in space, two coordinate systems will be defined. The coordinate system fixed in the disk will be denoted as the (r,θ) system, whereas that fixed in space will be denoted as the (r, γ) system. The radial coordinate r is the same in each case. These two coordinate systems and the physical dimensions of a perfect disk are shown in figure 1.

The disk rotational speed is Ω in the positive γ direction, and the origins of both angular coordinates are taken to be coincident at $t = 0$. Therefore a point located at an angle θ in the disk is located in space at an angle γ given by:

$$\gamma = \Omega t - \theta$$

Similarily, the reverse transformation is:

$$\theta = \Omega t - \gamma$$

The transverse displacement as a function of θ is denoted by w, and as a function of γ by u.

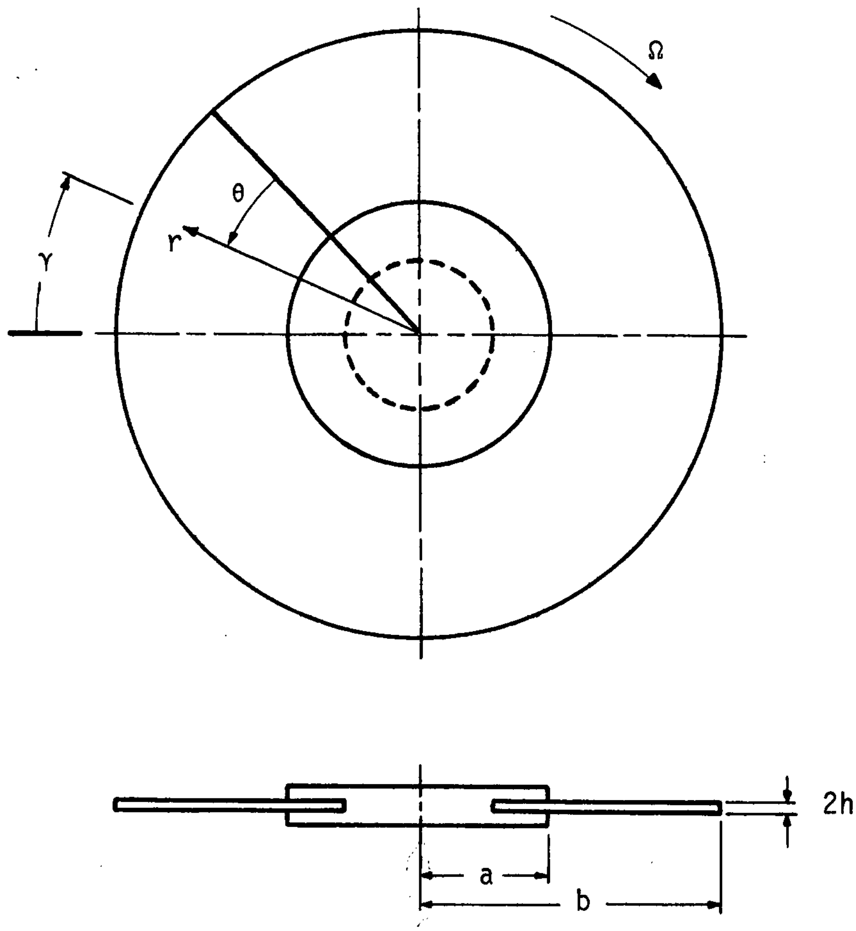

Figure 1

Perfect Disk Dimensions and Coordinate Systems

Initially the method of solution of the free vibrations of a perfect, centrally clamped non-rotating disk is outlined. The results obtained from this analysis form the basis for predicting the disk behaviour when the problem is compounded with imperfections, rotational stresses and a transverse load.

II.1 Free Response of a Perfect Non-rotating Disk

The equilibrium plate bending equation for a homogenous, isotropic plate is:[21]

(II.1) $$\nabla^4 w = q/D$$

Here q is the transverse load per unit area and D is the flexural rigidity given by:

$$D = E(2h)^3/12(1-\nu^2)$$

The biharmonic operator is to be expressed in polar coordinates.

For the case of a freely vibrating non-rotating disk, the only load is that due to the inertial forces and internal and external damping. If damping is neglected, equation (II.1) may be written as:

(II.2) $$\nabla^4 w = -\frac{\rho}{D}\frac{\partial^2 w}{\partial t^2}$$

There are four boundary conditions which the solution of equation (II.1) must satisfy. They are:

(a) no deflection at the clamp

(b) no slope at the clamp

(c) no internal radial bending moment at the free edge

(d) twisting moment/shear stress condition at the free edge (Kirchoff boundary condition)

A separation of variables form of a solution may be assumed in this case:

$$w = R(r)T(t)\Theta(\theta) \tag{II.3}$$

When equation (II.3) is substituted into equation (II.2), a suitable expression for Θ is found to be:

$$\Theta(\theta) = B_1 \cos n\theta + B_2 \sin n\theta \tag{II.4}$$

The necessity that $w(r,t,\theta) = w(r, t,\theta + 2\pi)$ requires that n is an integer. The expression for T is also immediately found to be of the form:

$$T(t) = C_1 \cos p_n t + C_2 \sin p_n t \tag{II.5}$$

The expressions for the natural frequencies p_n are unknown at this stage except that they are dependent on the integer n.

The solution as given by equation (II.3) may then be written as:

$$w_n = R(r)\,[B_1 \cos n\theta + B_2 \sin n\theta][C_1 \cos p_n t + C_2 \sin p_n t] \tag{II.6}$$

The subscript n now appears on w, indicating that there is a solution for each value of n selected.

In order to determine the radial function R(r) and the frequencies p_n, consider one term of equation (II.6), which may be written as:

$$w_n = A_n R(r) \sin n\theta \cos p_n t \tag{II.7}$$

After substituting equation (II.7) into the equation of motion, the function R(r) may be determined by solving two differential equations; Bessel's equation and the Modified Bessel's equation[5]. Equation (II.7) is then:

(II.8) $$w_n = [a_1 J_n + a_2 Y_n + a_3 I_n + a_4 K_n] \sin n\theta \cos p_n t$$

Here J_n, Y_n, I_n, and K_n are Bessel and Modified Bessel functions of the first and second kinds, whose arguments are dependent on D and p_n. Substitution of equation (II.8) into the boundary conditions yields a characteristic equation, from which the natural frequencies and radial functions may be determined. For a particular value of n there are an infinite number of frequencies and radial functions. Each of these radial functions may be identified by the number of values of r at which there is no transverse motion. These circles, excluding the central one due to the clamp, are called nodal circles, and the number of them occurring is denoted by s, where s = 0, 1, 2... . It may also be seen from equation (II.8) that there exists n diameters of zero transverse motion, known as nodal diameters. The s nodal circles, n nodal diameters response of equation (II.8) may be written as:

(II.9) $$w_{n,s} = A_{n,s} R_{n,s}(r) \sin n\theta \cos p_{n,s} t$$

For reasons which will become apparent when the forced response of a rotating disk is discussed, it is only the zero nodal circles modes which are of concern. The response of the disk in those modes where $s \neq o$ is therefore neglected and the subscript s may be ommitted. Equation (II.9) is then:

$$w_n = A_n R_n(r) \sin n\theta \cos p_n t$$

This expression, however, was developed by considering only one term of equation (II.6). When all four terms are considered the n nodal diameter response is:

$$w_n = R_n(r)\,[B_1C_1 \cos n\theta \cos p_n t + B_1C_2 \cos n\theta \sin p_n t + B_2C_1 \sin n\theta \cos p_n t + B_2C_2 \sin n\theta \sin p_n t]$$

It is possible to write this expression in two forms using the trigonometric identity:

$$a \sin x + b \cos x = c \cos (x - \zeta)$$

$$\text{where:} \quad a^2 + b^2 = c^2$$

$$\text{and} \quad \zeta = \tan^{-1} b/a$$

By applying this identity to the angular trigonometric terms we obtain:

(II.10) $$w_n = R_n(r)\,[A_{n1} \cos (n\theta-\theta_1) \sin p_n t + A_{n2} \cos (n\theta-\theta_2) \cos p_n t]$$

The second form is obtained by applying the identity to the temporal trigonometric terms:

(II.11) $$w_n = R_n(r)\,[A_{n1} \sin n\theta \cos (p_n t-\varepsilon_1) + A_{n2} \cos n\theta \cos (p_n t-\varepsilon_2)]$$

Equations (II.10) and (II.11) are the two forms of the n nodal free response of a perfect disk. Although they are equivalent, it is the form given by equation (II.11) which will be used for the remainder of this thesis for reasons which will become apparent when the response of an imperfect disk is considered.

There are four constants in equation (II.11) which must be determined from the initial conditions of the free response. It will now be shown that although this expression is referred to as the n nodal diameter response, it does not in general consist of what is commonly known as nodal diameters.

If we set $w_n = 0$ in equation (II.11), the following expression for θ results:

$$\tan n\theta = \frac{A_{n2}}{A_{n1}} \frac{\cos (p_n t - \varepsilon_2)}{\cos (p_n t - \varepsilon_1)}$$

From this expression it can be seen that, in general, the angular locations where the displacement is zero is a function of time. If, however, $\varepsilon_1 = \varepsilon_2$ this becomes:

$$\tan n\theta = - A_{n2} / A_{n1} = \text{constant}$$

which is the familar case of a free response with nodal diameters fixed in the disk. Referring to equation (II.11) it can be seen that this motion results when the disk is initially deformed in the shape $w_{n\text{-initial}} = R_n(r) \times [A_{n1} \sin n\theta + A_{n2} \cos n\theta]$ and released at $t = \varepsilon_1 / p_n$.

As a second example, if the temporal phase angles are such that $\varepsilon_2 = \varepsilon_1 + 3\pi/2$ and if $A_{n1} = A_{n2}$, the location of the nodal lines is given by:

$$\tan n\theta = \tan (p_n t - \varepsilon_1)$$

$$\theta = \frac{p_n t}{n} - \frac{\varepsilon_1}{n}$$

These nodal lines are travelling around the disk at a constant speed of $\dot{\theta} = p_n/n$. The initial conditions of this motion may be obtained by substituting $\varepsilon_2 = \varepsilon_1 + 3\pi/2$ into equation (II.11). Due to the difficulty in creating these initial conditions, this motion is not commonly observed experimentally.

Both of the above cases, the vibration fixed in the disk and the travelling wave, are special cases of the more general result. From equation (II.11) it can be seen that in general the n nodal diameter free response consists of two oscillating n nodal diameter shapes, with the nodes of one located half-way between those of the other. Although the frequencies are equal, the time phases are not.

II.2 Free Response of an Imperfect Non-rotating Disk

As previously discussed, an imperfect disk is here defined to be a disk whose geometry and physical properties differ slightly from those of the idealized perfect disk. While the effects of the imperfections could be determined quantitatively if the imperfections can be mathematically modelled, this is not likely to be the case. The following theoretical developments do not require such a knowledge of the nature of the imperfections, yet they provide very useful qualitative information.

The energy method is used here to investigate the effects of imperfections on the free vibrations of a non-rotating disk.[3] The assumed expression for the total free response is given by equation (II.12) where $\Phi(t)$ and $\Psi(t)$ are to be determined.

$$w = \sum_n [\Phi_n(t)\, R_n(r) \cos n\theta + \Psi_n(t)\, R_n(r) \sin n\theta] \qquad \text{(II.12)}$$

Two types of energy will be considered here; the kinetic energy of the transverse motion and the strain energy of deformation. The energy dissipated by damping is considered in a later section.

(i) Kinetic Energy: The kinetic energy of the transverse vibrations of the disk is given by:

$$T = \tfrac{1}{2} \int_{vol} \rho(\dot{w})^2\, r\,dr\,d\theta\,dz$$

From equation (II.12):

$$(\dot{w})^2 = \sum_n \sum_m R_n R_m\, [\dot{\Phi}_n \dot{\Phi}_m \cos n\theta \cos m\theta +$$

$$\dot{\Psi}_n \dot{\Psi}_m \sin n\theta \sin m\theta + 2\dot{\Phi}_n \dot{\Psi}_m \cos n\theta \sin m\theta]$$

Due to the orthogonality of the trigonometric terms in $(\dot{w})^2$, the only remaining terms after the kinetic energy integration would be those containing $\cos n\theta \cos m\theta$ and $\sin n\theta \sin m\theta$ for $n = m$.

In this case, the kinetic energy is of the form:

$$(II.13) \qquad T = \sum_n \tfrac{1}{2}\mu_n \dot{\Phi}_n^2 + \tfrac{1}{2}\mu_n \dot{\Psi}_n^2$$

where:

$$(II.14) \qquad \mu_n = 2\rho\pi h \int [R_n(r)]^2 \, r \, dr$$

This, however, assumes that the disk is perfect.

Although the imperfections are considered to be general in nature, as an illustrative example consider the case where the imperfection consists of a density variation in the angular direction. If the density can be represented as:

$$(II.15) \qquad \rho(\theta) = \sum_{k=0} C_k \cos k\theta + D_k \sin k\theta$$

the results of the kinetic energy integration will be somewhat different than in the perfect disk case. The integrand of the kinetic energy integral for this density imperfection is:

$$\begin{aligned}\rho(\dot{w})^2 r = \sum_k \sum_m \sum_n R_n R_m [&\dot{\Phi}_n\dot{\Phi}_m \cos n\theta \cos m\theta \; (C_k \cos k\theta + \\ &D_k \sin k\theta) + \dot{\Psi}_n\dot{\Psi}_m \sin n\theta \sin m\theta \; (C_k \cos k\theta + \\ &D_k \sin k\theta\,) \; + \; 2\,\dot{\Phi}_n\dot{\Psi}_m \cos n\theta \sin m\theta \; x \\ &(C_k \cos k\theta + D_k \sin k\theta\,)]r\end{aligned}$$

Of the six terms within this summation, it cannot be said that any one will vanish for all values of k, m, and n when the integration is performed over the range of θ. If, however, the density imperfections are small, all values of C_k and D_k in equation (II.15) are also small with the exception of C_o.

The general form of the kinetic energy expression is then:

(II.16)

$$T = \tfrac{1}{2} \sum_m \sum_n a_{nm} \dot{\Phi}_n \dot{\Phi}_m + 2\, c_{nm} \dot{\Phi}_n \dot{\Psi}_m + b_{nm} \dot{\Psi}_n \dot{\Psi}_m$$

where a_{nm} and b_{nm} are small for $n \neq m$, and c_{nm} is small for all n and m. In addition, the values of a_{nm} and b_{nm}, for $n = m$, are slightly different from what they would be for a perfect disk.

(ii) Strain Energy: For a non-rotating disk, the strain energy is that due to bending. In polar-cylindrical coordinates this is:[6]

$$U = \iiint_{vol} \frac{E\, z^2}{2(1-\nu^2)} \left\{ \left(\frac{\partial^2 w}{\partial r^2} + \frac{1}{r}\frac{\partial w}{\partial r} + \frac{1}{r^2}\frac{\partial^2 w}{\partial \theta^2}\right)^2 \right.$$

$$\text{(II.17)} \quad - 2(1-\nu)\, \frac{\partial^2 w}{\partial r^2} \left(\frac{1}{r}\frac{\partial w}{\partial r} + \frac{1}{r^2}\frac{\partial^2 w}{\partial \theta^2}\right)$$

$$\left. + 2(1-\nu) \left[\frac{\partial}{\partial r}\left(\frac{1}{r}\frac{\partial w}{\partial \theta}\right)\right]^2 \right\} r\,dr\,d\theta\,dz$$

If the disk is considered to be perfect, the resulting expression for the strain energy is:

$$\text{(II.18)} \quad U = \sum_n \tfrac{1}{2} \beta_n \Phi_n^2 + \tfrac{1}{2} \beta_n \Psi_n^2$$

where:

$$\beta_n = \frac{Eh^3\pi}{3(1-\nu^2)} \int \left\{ \left(\frac{d^2R}{dr^2}\right)^2 + 2\nu\left(\frac{1}{r}\frac{dR}{dr} - \frac{n^2}{r^2} R\right) \frac{d^2R}{dr^2} \right.$$

$$+ \frac{1}{r^2}\left[1 + 2n\ (1-\nu)\right] \left(\frac{dR}{dr}\right)^2 - \frac{2n^2R}{r^3}\left[1 + 2(1-\nu)\right]\frac{dR}{dr}$$

(II.19)

$$\left. + \frac{1}{r^4}\left[n^4 + 2n^2(1-\nu)\right] R^2 \right\} rdr$$

Here R denotes $R_n(r)$. As can be seen from equation (II.17),each term of the strain energy integrand contains either cos mθ cos nθ, sin nθ sin mθ or cos nθ sin mθ. Again, due to the orthogonality of the trigonometric terms, no cross-terms appear in the strain energy expression for a perfect disk. However, if the disk is imperfect, the general form of the strain energy is:

(II.20)

$$U = \tfrac{1}{2} \sum_m \sum_n \bar{a}_{nm} \Phi_n\Phi_m + 2\,\bar{c}_{nm} \Phi_n\Psi_m + \bar{b}_{nm} \Psi_n\Psi_m$$

Here the relative magnitudes of $\bar{a}_{nm}$, $\bar{c}_{nm}$ and $\bar{b}_{nm}$ are similar to those of a_{nm}, c_{nm} and b_{nm}.

Lagrange's equations for the free undamped vibrations of this system are:[6]

$$\frac{d}{dt}\left(\frac{\partial T}{\partial \dot{\Phi}_i}\right) + \frac{\partial U}{\partial \Phi_i} = 0$$

$$\frac{d}{dt}\left(\frac{\partial T}{\partial \dot{\Psi}_i}\right) + \frac{\partial U}{\partial \Psi_i} = 0$$

The results of substituting equations (II.16) and (II.20) into Lagrange's equations are:

$$\sum_m a_{nm} \ddot{\Phi}_m + \bar{a}_{nm} \Phi_m + c_{nm} \ddot{\Psi}_m + \bar{c}_{nm} \Psi_m = 0 \tag{II.21}$$

$$\sum_m b_{nm} \ddot{\Psi}_m + \bar{b}_{nm} \Psi_m + c_{nm} \ddot{\Phi}_m + \bar{c}_{nm} \Phi_m = 0 \tag{II.22}$$

Here there are two systems of linear differential equations, each system consisting of an infinite number of equations, one equation for each value of n.

By the theory of systems of linear differential equations with constant coefficients[23], solutions are sought of the form $\Phi_j = X_j e^{\lambda t}$ and $\Psi_j = Y_j e^{\lambda t}$. However, λ must be pure imaginary since the system is conservative.[2] The assumed form of the solutions to equations (II.21) and (II.22) are therefore taken as:

$$\begin{aligned} \Phi_j &= X_j \cos(\omega t - \gamma) \\ \Psi_j &= Y_j \cos(\omega t - \gamma) \end{aligned} \tag{II.23}$$

These assumed solutions may be substituted into each of the equations of (II.21) and (II.22). The result, for example, of substituting into the n=2 equation of (II.21) is:

$$\begin{aligned} &(\bar{a}_{21} - \omega^2 a_{21}) X_1 + (\bar{a}_{22} - \omega^2 a_{22}) X_2 + \text{---} \\ &+ (\bar{c}_{21} - \omega^2 c_{21}) Y_1 + (\bar{c}_{22} - \omega^2 c_{22}) Y_2 + \text{---} = 0 \end{aligned}$$

All such resulting equations may be written in matrix form as:

(II.24)

$$\begin{bmatrix} (\bar{a}_{11}-\omega^2 a_{11}) & (\bar{c}_{11}-\omega^2 c_{11}) & (\bar{a}_{12}-\omega^2 a_{12}) & (\bar{c}_{12}-\omega^2 c_{12}) & --- \\ (\bar{c}_{11}-\omega^2 c_{11}) & (\bar{b}_{11}-\omega^2 b_{11}) & (\bar{c}_{12}-\omega^2 c_{12}) & (\bar{b}_{12}-\omega^2 b_{12}) & --- \\ (\bar{a}_{21}-\omega^2 a_{21}) & (\bar{c}_{21}-\omega^2 c_{21}) & (\bar{a}_{22}-\omega^2 a_{22}) & (\bar{c}_{22}-\omega^2 c_{22}) & --- \\ (\bar{c}_{21}-\omega^2 c_{21}) & (\bar{b}_{21}-\omega^2 b_{21}) & (\bar{c}_{22}-\omega^2 c_{22}) & (\bar{b}_{22}-\omega^2 b_{22}) & --- \\ \vdots & \vdots & \vdots & \vdots & \end{bmatrix} \begin{Bmatrix} X_1 \\ Y_1 \\ X_2 \\ Y_2 \\ \vdots \end{Bmatrix} = \begin{Bmatrix} 0 \\ 0 \\ 0 \\ 0 \\ \vdots \end{Bmatrix}$$

or:

(II.25)
$$[\tilde{M}]\{\tilde{A}\} = \{\tilde{0}\}$$

A non-trivial solution to equation (II.25) exists if and only if $\det[\tilde{M}] = 0$. In the case where the imperfections are small, the non-diagonal elements of the matrix $[\tilde{M}]$ are small in relation to the diagonal elements. The solutions to the equation $\det[\tilde{M}] = 0$ are then approximately determined by solving:

$$(\bar{a}_{11} - \omega^2 a_{11})(\bar{b}_{11} - \omega^2 b_{11})(\bar{a}_{22} - \omega^2 a_{22})(\bar{b}_{22} - \omega^2 b_{22}) --- = 0$$

The values of ω which are the solutions to this equation will be denoted by p and q:

(II.26)
$$p_1^2 = \bar{a}_{11}/a_{11} \quad , \quad p_2^2 = \bar{a}_{22}/a_{22} \quad \cdots\cdot$$
$$q_1^2 = \bar{b}_{11}/b_{11} \quad , \quad q_2^2 = \bar{b}_{22}/b_{22} \quad \cdots\cdot$$

where $p_i \simeq q_i$; since $a_{ii} \simeq b_{ii}$ and $\bar{a}_{ii} \simeq \bar{b}_{ii}$.

Each eigenvalue of equations (II.26) , p_i or q_i , may be substituted into equation (II.24) from which the relative magnitudes of the components of the matrix $\{\tilde{A}\}$ may then be determined. For example, the assumed solutions, equations (II.23), obtained by putting $\omega = p_1$ in equation (II.24) may be written as:

$$\Phi_1 = P_{11}\cos(p_1 t - \varepsilon_1) \qquad \Psi_1 = B_{11}\cos(p_1 t - \varepsilon_1)$$
$$\Phi_2 = P_{21}\cos(p_1 t - \varepsilon_1) \qquad \Psi_2 = B_{21}\cos(p_1 t - \varepsilon_1)$$
$$\vdots \qquad\qquad\qquad\qquad \vdots$$

Here $P_{11}, P_{21}\ \ldots,\ B_{11}, B_{21}\ \ldots$ and ε_1 denote $X_1, X_2\ \ldots,\ Y_1, Y_2\ \ldots$ and γ as determined for $\omega = p_1$. For $\omega = p_i$ and $\omega = q_i$, Φ_j and Ψ_j may be written as:

$$\text{(II.26)} \qquad \Phi_j = P_{ji}\cos(p_i t - \varepsilon_i) \quad ; \quad Q_{ji}\cos(q_i t - \zeta_i)$$

$$\text{(II.27)} \qquad \Psi_j = B_{ji}\cos(p_i t - \varepsilon_i) \quad ; \quad D_{ji}\cos(q_i t - \zeta_i)$$

The most general forms of the solutions for Φ_j and Ψ_j are the sums of the solutions given by equations (II.26) and (II.27):

$$\text{(II.28)} \qquad \begin{aligned} \Phi_j &= \sum_i \left\{P_{ji}\cos(p_i t - \varepsilon_i) + Q_{ji}\cos(q_i t - \zeta_i)\right\} \\ \Psi_j &= \sum_i \left\{B_{ji}\cos(p_i t - \varepsilon_i) + Q_{ji}\cos(q_i t - \zeta_i)\right\} \end{aligned}$$

With a change of the dummy indices i and j , equations (II.28) may be substituted into the initial expression for the free vibration, equation (II.12), yielding:

$$w = \sum_m \Big\{ R_m(r) \cos m\theta \sum_n \big[P_{mn} \cos(p_n t - \varepsilon_n) + Q_{mn} \cos(q_n t - \zeta_n)\big] +$$
$$R_m(r) \sin m\theta \sum_n \big[B_{mn} \cos(p_n t - \varepsilon_n) + D_{mn} \cos(q_n t - \zeta_n)\big] \Big\}$$

It is possible to rearrange this expression to identify the shape of the response at a frequency p_n (or q_n). If we denote by w_{n1} (w_{n2}) the response at the frequency p_n (q_n), the result is:

$$w_{n1} = \cos(p_n t - \varepsilon_n) \sum_m \big[P_{mn} R_m \cos m\theta + B_{mn} R_m \sin m\theta\big]$$

(II.29)

$$w_{n2} = \cos(q_n t - \zeta_n) \sum_m \big[Q_{mn} R_m \cos m\theta + D_{mn} R_m \sin m\theta\big]$$

Clearly the effects of the imperfections are to not only alter the natural frequencies, but to also alter the shapes of the modes. If the coefficients a_{mn}, b_{mn} ... are known, it is possible to determine the relative magnitudes of P_{mn}, B_{mn} and Q_{mn}, D_{mn} and hence evaluate the natural frequencies and mode shapes ("The Theory of Sound", § 90)[2]. It can also be shown that the contribution of the cos mθ shape to that of the n nodal diameter mode is proportional to $\left(\frac{-1}{p_{*m}^2 - p_{*n}^2}\right)$ w, where here p_{*m} and p_{*n} are the natural frequencies of a perfect disk. If it is assumed that this contribution is negligable, that is, that the imperfection does not alter the actual shapes of the modes of vibration, equations (II.29) are:

$$(II.30) \qquad w_{n1} = R_n \cos(p_n t - \varepsilon_n)\,[P_{nn} \cos n\theta + B_{nn} \sin n\theta]$$

$$w_{n2} = R_n \cos(q_n t - \zeta_n)\,[Q_{nn} \cos n\theta + D_{nn} \sin n\theta]$$

The two independent expressions for the n nodal diameter free vibrations of the disk are those given by equations (II.29), or approximately by equations (II.30). Equations (II.30) may be written as:

$$(II.31) \qquad w_{n_1} = R_n \,\phi_n \cos(n\theta - \alpha_n)$$

$$w_{n2} = R_n \,\psi_n \sin(n\theta - \beta_n)$$

where $\phi_n = \sqrt{P_{nn}^2 + B_{nn}^2}\,\cos(p_n t - \varepsilon_n)$

$\psi_n = \sqrt{Q_{nn}^2 + D_{nn}^2}\,\cos(q_n \;\; - \zeta_n)$

and $\alpha_n = \tan^{-1} B_{nn} / P_{nn}$

$\beta_n = -\tan^{-1} Q_{nn} / D_{nn}$

If it is assumed that the imperfections do not alter the shape of the response, the coordinates ϕ_n and ψ_n are the disk normal coordinates, since a free vibration is possible which is characterized by the vanishing of all ϕ_n and ψ_n except one.[2,3] When the kinetic and strain energies of the imperfect disk are expressed in terms of these normal coordinates, the coefficients of the cross-terms must be zero. By comparing the expressions for Φ_n, Ψ_n, ϕ_n and ψ_n the relationships between the two sets of coordinates is seen to be:

$$\Phi_n = \phi_n \cos \alpha_n - \psi_n \sin \beta_n$$

$$\Psi_n = \phi_n \sin \alpha_n + \psi_n \cos \beta_n$$

Upon substitution of these equations into the kinetic and strain energy equations, (II.16) and (II.20), there results the following:

$$2T = A_n \dot{\phi}_n^2 + B_n \dot{\psi}_n^2 + C_n \dot{\phi}_n \dot{\psi}_n$$

$$2U = \bar{A}_n \phi_n^2 + \bar{B}_n \psi_n^2 + \bar{C}_n \phi_n \psi_n \qquad \text{(II.32)}$$

The coefficients A_n, B_n etc. are functions of the angles α_n and β_n as well as the coefficients a_{nn}, b_{nn} etc. Setting the coefficients of the cross-terms, that is C_n and $\bar{C}_n$, to zero results in the following expressions for α_n and β_n:

$$(b\bar{c} - c\bar{b}) \tan^2\alpha_n + (b\bar{a} - a\bar{b}) \tan \alpha_n + (c\bar{a} - a\bar{c}) = 0$$

$$(c\bar{a} - a\bar{c}) \tan^2\beta_n - (b\bar{a} - a\bar{b}) \tan \beta_n + (b\bar{c} - c\bar{b}) = 0 \qquad \text{(II.33)}$$

The sub-scripts "nn" have been ommitted. In addition to the above two expressions for α_n and β_n, their ratio is obtained as:

$$\frac{\tan \alpha_n}{\tan \beta_n} = \frac{\bar{c}a - \bar{a}c}{\bar{c}b - \bar{b}c} \qquad \text{((II.34)}$$

Lagrange's equation may be used with the expressions for T and U, equations (II.32), to determine the natural frequencies. This results in:

$$p_n^2 = \frac{\bar{a} + \bar{b}\tan^2\alpha_n + 2\bar{c}\tan\alpha}{a + b\tan^2\alpha_n + 2c\tan\alpha} \qquad \text{(II.35)}$$

$$q_n^2 = \frac{\bar{b} + \bar{a}\tan^2\beta_n - 2\bar{c}\tan\beta_n}{b + a\tan^2\beta_n - 2c\tan\beta_n}$$

Equations (II.33), (II.34) and (2.35) require, for their use, an exact knowledge of the imperfections. This is not likely to be known except in the simplest of cases.

However, several significant results are available from these equations. From equations (II.35), it is seen that p_n (q_n) is a function of α_n (β_n), and also a, b etc. which are constants dependent solely on the disk physical characteristics. If stationary values of p_n or q_n are sought, the resulting expressions for α_n and β_n are those given by equations (II.33). That is, the nodal lines, determined by α_n and β_n, are located such that the frequencies p_n and q_n are stationary in value.

However, for a perfect disk, where $a_{nn} = b_{nn}$, $\bar{a}_{nn} = \bar{b}_{nn}$ and $c_{nn} = \bar{c}_{nn} = 0$, equations (II.35) show that $p_n = q_n$ regardless of the values of α_n or β_n.

A second result regarding α_n and β_n is available from equations (II.33) and (II.34). Clearly, for a perfect disk, both of these expressions for α_n and β_n are indeterminant, and hence the location of the nodes cannot be determined solely from the disk physical characteristics. In the case where the disk is imperfect but the nature of the imperfections is such that their influence on the kinetic energy is much greater than on the strain energy, equations (II.33) may be written approximately as:

$$-c \tan^2\alpha_n + (b - a) \tan \alpha_n + c = 0$$

$$-c \tan^2\beta_n + (a - b) \tan \beta_n + c = 0$$

When their influence on the strain energy predominates:

$$-\bar{c} \tan^2\alpha_n + (\bar{b} - \bar{a}) \tan \alpha_n + \bar{c} = 0$$

$$-\bar{c} \tan^2\beta_n + (\bar{a} - \bar{b}) \tan \beta_n + \bar{c} = 0$$

In either case it can be seen that the extent to which the angles α_n and β_n differ is greater for greater imperfections within the disk.

The free vibrations of a disk with small imperfections may be taken as:

$$w = \sum_n \Big[A_{n1} R_n \cos (n\theta - \alpha_n) \cos (p_n t - \varepsilon_n) + A_{n2} R_n \sin (n\theta - \beta_n) \cos (q_n t - \zeta_n)\Big] \tag{II.36}$$

where the differences between α_n, β_n and p_n, q_n in general depend on the nature and extent of the imperfections, and where α_n and β_n are such that p_n and q_n are stationary in value.

The two terms of equation (II.36), that is:

$$w_{n1} = A_{n1} R_n \cos (n\theta - \alpha_n) \cos (p_n t - \varepsilon_n)$$

$$w_{n2} = A_{n2} R_n \sin (n\theta - \beta_n) \cos (p_n t - \zeta_n)$$

are referred to as the two configurations of the n - nodal diameter vibration. Each is independent of the other, that is, each is a mode of vibration, and the amplitudes, A_{n1} and A_{n2}, and the time phases, ε_n and ζ_n, are dependent entirely on the initial conditions.

It should be pointed out that there are very special cases where imperfections may be present and either the phase angles α_n and β_n are equal, or the frequencies p_n and q_n are equal. As an example of the first case, consider a mass imperfection symmetric about some angular location on the disk. Any free vibration must also be symmetric about that point. This requires that a node of one configuration and an anti-node of the other pass through the point. Since the shapes of the configurations are assumed to be unaltered, it must be that $\alpha_n = \beta_n$. As an example of the second case, if the imperfections are symmetric about m equally spaced locations on the disk, the requirement that p_n and q_n be stationary in value results in $p_n = q_n$ when 2n is not an integer multiple of m. This second case is known as the Zenneck rule.[13]

Although either the difference between α_n and β_n, or between p_n and q_n could be considered measures of the imperfection of a disk, it is the latter that is the accepted practice.

While it is possible to experimentally determine the coefficients a_n, b_n etc., this would be extremely difficult to do. Since the desired information is the natural frequencies p_n and q_n and the location of the nodes, these can be determined directly and with much greater ease by experimental methods which are described later.

It is, however, desirable to obtain numerical results so that theoretical predictions can be compared with experimental results. It is found that theoretical results based on a perfect disk assumption and adjusted according to information obtained experimentally from the free response of an imperfect disk predicts a forced response that is consistent with experimental evidence.

The following section gives an approximate method whereby numerical results for the free vibrations of a perfect non-rotating disk may be obtained.

II.3 An Approximate Method of Determining the Free Vibrations of a Non-rotating Disk

The natural frequencies of a non-rotating disk may be determined by several different approaches. One, previously mentioned, requires solving the equation of motion for the radial functions $R_n(r)$. The result of requiring the radial functions to conform to the boundary conditions yields the natural frequencies and the relative magnitudes of the coefficients of the Bessel and Modified Bessel functions.

Another possible approach is that known as the Rayleigh-Ritz method. This is the approach which will be taken here. In order to use the Rayleigh-Ritz method, the shape of the vibration must be represented as a kinematically admissible orthogonal sequence with unknown coefficients. Using this shape an expression for the natural frequencies may be obtained. This expression is a function of the unknown coefficients, and minimizing the frequency with respect to these coefficients yields an upper bound on the fundamental frequency of the free vibration.

It is not necessary to assume an angular shape, however, since it is known to consist of nodal diameters which must be symmetrically distributed around the disk. It is the radial functions $R_n(r)$ which are unknown. A kinematically admissible representation of the radial functions is:[5]

$$R_n(r) = \left(\frac{r-a}{b-a}\right)^2 \sum_{k=0}^{\infty} \tau_k \left(\left(\frac{r-a}{b-a}\right)\right)^k$$

Here the τ_k are the unknown coefficients.

The value of this function and its slope are both zero at the clamp as required. If only the first two terms are taken, the approximation to the radial function is:

$$R_n(\chi) = \tau_0 \chi^2 + \tau_1 \chi^3 \qquad \chi = \left(\frac{r-a}{b-a}\right)$$

The range of χ is then $0 \leqslant \chi \leqslant 1$. Since $R_n(\chi)$ may be multiplied by a constant without affecting the result in any way, we can write:

$$R_n(\chi) = \chi^2 + \tau \chi^3 \tag{II.37}$$

Because the angular function is known exactly, if the frequency is determined by use of the radial function given by equation (II.37) then minimized with respect to τ, the resulting minimum is an upper bound on the natural frequency of that n nodal diameters, zero nodal circles mode.

The expressions for the kinetic and strain energies as previously given by equations (II.13) and (II.18) are:

$$2T = \mu_n \; \Phi\dot{\Phi}_n^2 + \mu_n \; \dot{\Psi}_n^2$$

$$2U = \beta_n \; \Phi_n^2 + \beta_n \; \Psi_n^2$$

where the values of μ_n and β_n are determined from the integrals of equations (II.14) and (II.19).

If damping is neglected and a harmonic time function is assumed, equating the maximum kinetic and strain energies results in an expression of the form:

$$p_n = \left[\frac{Eh^2}{\rho b^4}\right]^{1/2} \left[\frac{S_1 \tau^2 + S_2 \tau + S_3}{K_1 \tau^2 + K_2 \tau + K_3}\right]$$

The coefficients S_1, S_2, and S_3 result from the strain energy calculation whereas K_1, K_2 and K_3 result from the kinetic energy calculation. All coefficients are functions of the disk dimensions a and b, Poisson's ratio, and the integer n. The value of τ which minimizes p_n is available in closed form in this case. It is possible to express the minimum value of p_n as:

$$p_n = \left[\frac{Eh^2}{\rho b^4}\right]^{\frac{1}{2}} \lambda$$

The exact values of λ have been determined by other means,[17] and are shown in figure 2 (solid lines) along with the values calculated by

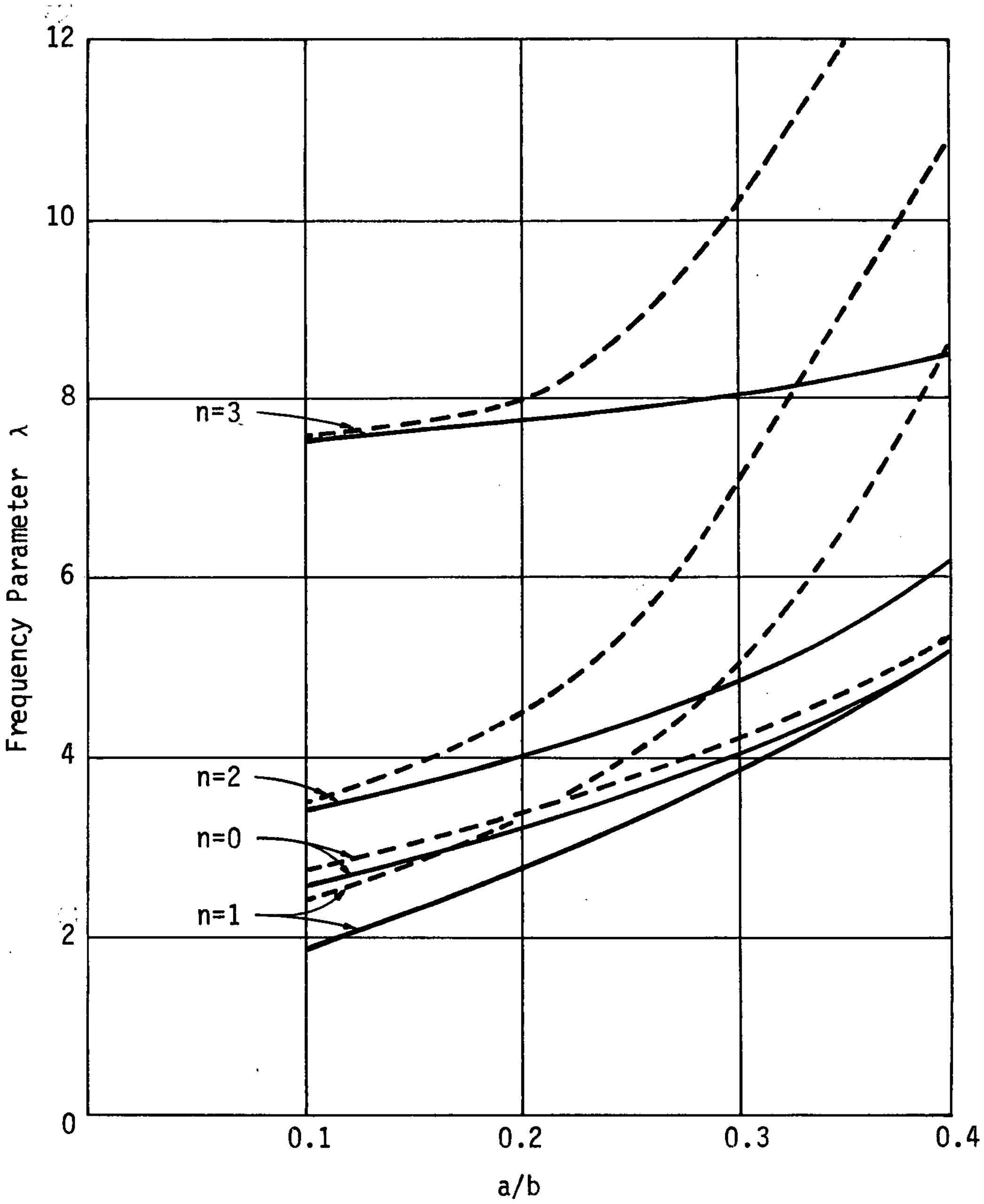

Figure 2

Non-dimensional Frequency Parameter versus Clamping Ratio the Rayleigh-Ritz method (dashed lines).

The Rayleigh-Ritz values of λ are generally more accurate for low values of the clamping ratio a/b, with the exception of the n = 0 mode whose error is essentially independent of the clamping ratio. For values of the clamping ratio greater than approximately 0.2, the use of only two terms for the approximating function is obviously insufficient.

The values of the coefficient τ which minimizes the frequencies p_n are given in figure 3. Using these values of τ it is possible to approximate the shape of the free vibrations of a perfect disk. However, this approximation neglects two effects which must be included in order to arrive at a useful result. The first is the previously discussed effect of imperfections which are treated experimentally in a later chapter. The second effect is that of the rotational stresses, which will now be discussed.

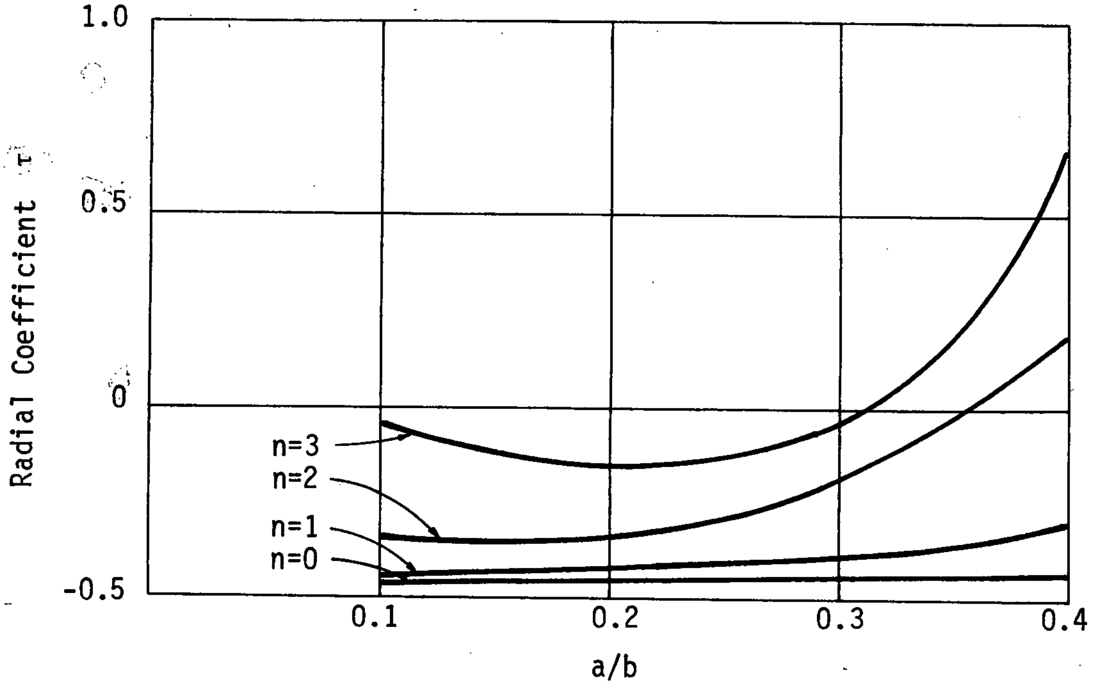

Figure 3

Radial Funtion Coefficient versus Clamping Ratio

II.4 The Effects of Rotation

The effects of rotation considered here are those attributable to the tensile membrane stresses which exist when the disk is rotating. Initially the influence of these stresses on the free vibrations of a perfect disk are investigated, then an approximate method is described by which this influence on the free vibrations of an imperfect disk may be included.

Rotating Membrane

In order to introduce the effects of rotational stresses, it is convenient to consider a rotating disk with no flexural rigidity; that is, a membrane. This approach will also be useful in a later section, where an empirical relationship for the effects of rotation will be presented.

The equilibrium equation for a non-vibrating, rotating circular membrane is obtained from the free-body diagram shown in figure 4. Due to symmetry there are no shear stresses, and the hoop stresses σ_θ are constant around the disk. The body force B is of magnitude $\Omega^2 r dm$ where dm is the mass of the element. The boundary conditions on the stress distribution are:

1. zero radial stress at the clamp.
2. zero radial stress at the free edge.

The first boundary condition is for what is referred to as a partial clamp. This type of clamp (or collar) is the type commonly found in practice. It allows a radial displacement of all points on the disk, and serves only to prevent a transverse displacement at the collar.

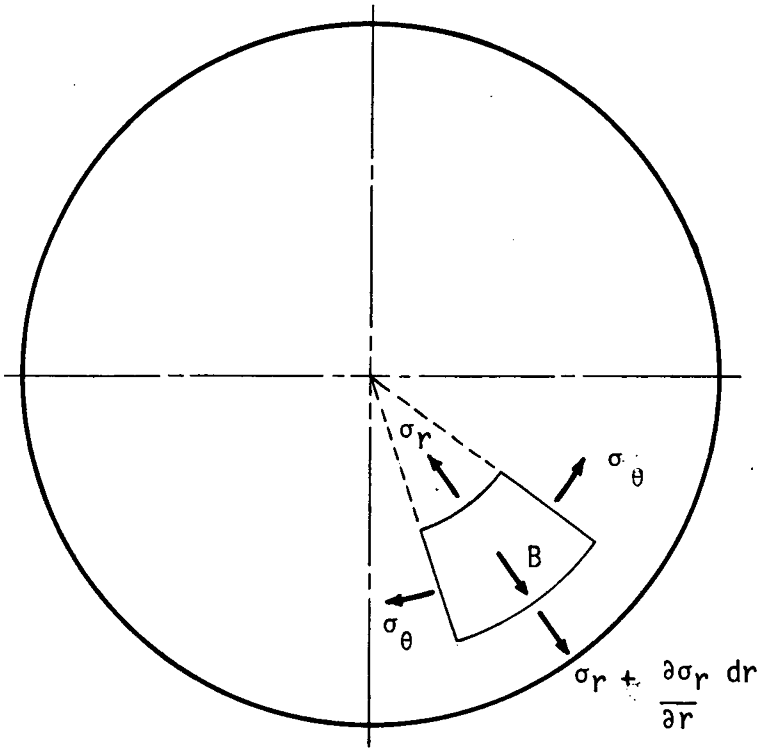

Figure 4
Membrane Stresses in a Rotating Membrane

With these boundary conditions the membrane stresses at any point may be determined. They are:[18]

$$\sigma_r = \left(\frac{k_2}{r^2}\right)\left[r^2 + \left(\frac{k_1}{b^2 k_2}\right)\right](b^2 - r^2)\ \rho\omega^2$$

$$\sigma_\theta = \left(\frac{k_2}{r^2}\right)\left\{\left[b^2 - \left(\frac{k_1}{b^2 k_2}\right)\right] r^2 - \left(\frac{k_1}{k_2}\right) - \left(\frac{k_3}{k_2}\right) r^4\right\} \rho\omega^2$$

where k_1, k_2 and k_3 are functions of the disk and collar radii and Poisson's ratio.

It is now assumed that the membrane is deformed arbitrarily in the transverse direction, but that the stresses do not change, as shown in figure 5.

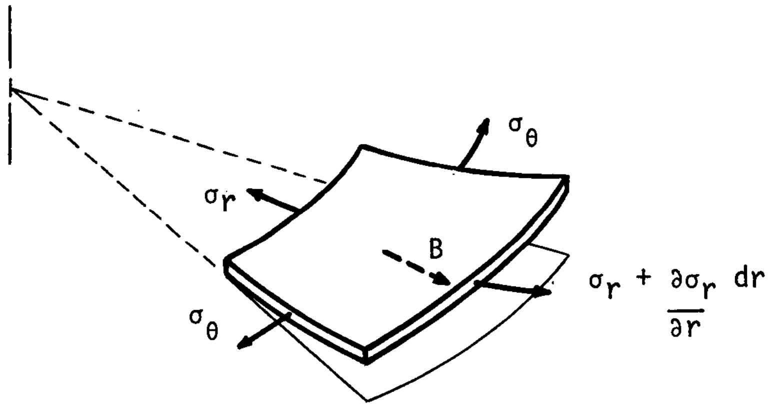

Figure 5

Deformed Element of a Rotating Membrane

As can be seen, on each element there is a net restoring force in the transverse direction, due in the radial case to both the variation in the radial stress and to the curvature in the radial direction, and in the angular case due to the curvature only. This net restoring force may be equated to the rate of change of momentum of the element, resulting in the equation of motion:

$$\frac{1}{r}\,\frac{\partial}{\partial r}\left(r\sigma_r\,\frac{\partial w}{\partial r}\right) + \frac{1}{r^2}\,\frac{\partial}{\partial \theta}\left(\sigma_\theta\,\frac{\partial w}{\partial \theta}\right) - \rho\,\frac{\partial^2 w}{\partial t^2} = 0$$

The boundary conditions on the transverse displacement are:

1. zero transverse displacement at the collar.
2. finite transverse displacement at the free edge.

The method of solving this differential equation is very lengthy, but numerical results are available.[18] The resulting expression for the transverse vibrations are of the same form as given in equation (II.9), but the radial functions are not the same. A significant result is that for a given disk the natural frequencies are directly proportional to the disk rotational speed. That is:

$$p_n^2 = V_n \Omega^2 \qquad \text{(II.38)}$$

where V_n is a function of n and the disk physical properties and dimensions.

Rotating Disk

It is possible to formulate the differential equation for a rotating disk considering both rotational and bending stresses using information previously presented. Equation (II.1), the plate bending equation, is the equilibrium equation for a non-rotating disk subjected to a transverse load, which was taken to be the inertial forces in the free vibrations case. However, the stresses due to rotation were seen to cause a net transverse load when the membrane was deformed. Therefore it is possible to use the plate bending equation for a rotating disk, where the transverse load is due to both the inertial forces and the rotational stresses. The resulting equation of motion is:

$$\mathbb{D}\,\nabla^4 w = \frac{1}{r}\;\frac{\partial}{\partial r}\left(r\,\sigma_r\,\frac{\partial w}{\partial r}\right) + \frac{1}{r^2}\,\frac{\partial}{\partial \theta}\left(\sigma_\theta\,\frac{\partial w}{\partial \theta}\right) - \rho\,\frac{\partial^2 w}{\partial t^2}$$

This equation was solved numerically by Eversman and Dodson and the results published in 1969.[19] The shape of the vibration is again found to consist of nodal circles and diameters, but the radial functions are different from those in either the non-rotating disk or rotating membrane cases.

As would be expected, the effects of the rotational stresses are dependent upon the clamping ratio a/b, the disk thickness and the rotational speed. It is found, however, that the influence of these stresses on the disk natural frequencies is not very large for disks and clamping ratios of the dimensions corresponding to those typical of circular saws. As an example, using results from the paper by Eversman and Dodson, an 18" diameter disk, 0.150" thick with an 8" diameter collar has a natural frequency of 198 Hz. for $n = 1$ when the disk is stationary, as compared to 237 Hz. at a rotational speed of 5300 r.p.m. This is an increase of only 19.5% which is in fact an upper limit since typical rotational speeds of circular saws are somewhat lower than 5300 r.p.m.

Under these conditions, reasonably accurate results may be obtained by an approximate method based on Southwell's Theorem.

Southwell's Theorem[4]

Southwell's Theorem is general in nature, not pertaining specifically to rotating disks. It is derived directly from Rayleigh's Theorem, which states that the natural frequency of the fundamental mode of vibration, as calculated from an assumed shape of deflection, is an upper bound for the exact value. In order to develop Southwell's Theorem as it applies to rotating disks, three deflection shapes must be defined:

S_T ... resulting from membrane and bending stresses

S_B ... resulting from bending stresses only (no rotation)

S_M ... resulting from membrane stresses only (no flexural rigidity)

Assuming simple harmonic motion, the maximum strain and kinetic energies of the transverse vibration may be written as:

$$\text{Strain Energy} = U\ (S)$$

$$\text{Kinetic Energy} = p^2\ T\ (S)$$

If damping is neglected, the frequency is given by:

$$p^2 = \frac{U\ (S)}{T\ (S)}$$

For small deflections, the work done by the bending stresses is independent of that done by the membrane stresses. Therefore:

$$U\ (S_T) = U_B\ (S_T) + U_M\ (S_T)$$

Where U_B and U_M are the bending and membrane potential energies. The frequency is then:

$$p_T^2 = \frac{U_B\ (S_T) + U_M\ (S_T)}{T\ (S_T)}$$

$$= \bar{p}_B^2 + \bar{p}_M^2$$

Here $\bar{p}_B$ and $\bar{p}_M$ are what the natural frequencies would be if the disk was assumed to vibrate in the shape S_T under the action of either the bending or the membrane stresses.

That is:

$$\bar{p}_B^2 = \frac{U_B\ (S_T)}{T\ (S_T)}$$

$$\bar{p}_M^2 = \frac{U_M\ (S_T)}{T\ (S_T)}$$

However, if only bending stresses or only membrane stresses were present, the shape would be S_B or S_M respectively. Therefore the exact values of p_B and p_M are given by:

$$p_B^2 = \frac{U_B\ (S_B)}{T\ (S_B)}$$

$$p_M^2 = \frac{U_M\ (S_M)}{T\ (S_M)}$$

By Rayleigh's Theorem, for the fundamental mode:

$$\bar{p}_B^2 \geqslant p_B^2$$

$$\bar{p}_M^2 \geqslant p_M^2$$

Therefore the expression for the frequency p_T becomes:

(II.39) $$p_T^2 \geqslant p_B^2 + p_M^2$$

Equation (II.39) is Southwell's Theorem. It can ben seen that if the potential energy of a freely vibrating body is due to the action of two (or more) systems of stresses which act independently, then a lower bound on the natural frequency of the fundamental mode may be determined by considering the effect of each system separately.

Equation (II.39) may serve as the basis for an empirical relationship if the equality is taken to hold:

$$p_T^2 = p_B^2 + p_M^2$$

However, equation (II.38) indicated that the relationship between p_M^2 and Ω was:

$$p_M^2 = V\Omega^2$$

Therefore:

$$p_T^2 = p_B^2 + V\Omega^2 \qquad \text{(II.40)}$$

In the previous example of the 0.150" disk, the increase in the n = 1 mode natural frequency in going from 0 to 5300 r.p.m. was 19.5%. If the exact value of V is used,[18] the increase is found to be 17% (232 Hz.) by equation (II.40). The actual difference in the 5300 r.p.m. natural frequency by the two methods is only 2%.

Evidently, for disks of the physical dimensions similar to those typical of circular saws, equation (II.40) provides a satisfactory approximation for the natural frequencies as a function of rotational speed.

While the coefficient V_n is available from the literature, there are several factors in practice which can significantly alter its value from that calculated theoretically. However, it may be approximated quite easily experimentally. Since for a real disk there will likely be two natural frequencies associated with the n nodal diameter free vibration, there would be two relationships of the form of equation (II.40):

$$p_T^2 = p_B^2 + V_{n_1}\Omega^2$$

$$q_T^2 = q_B^2 + V_{n_2}\Omega^2$$

Experimentally determining the coefficients V_n necessitates observing the disk natural frequencies at various rotational speeds. However, observations will generally be made from points stationary in space, whereas the equations describing the transverse motion have been given with respect to a coordinate system fixed in the disk. The following section therefore describes the results of the transformation to a coordinate system fixed in space.

II.5 Disk Displacement with Respect to Rotating and Non-rotating Coordinates

The significance of the difference between the observed disk displacement as expressed in terms of the rotating or non-rotating coordinate systems may be illustrated by considering the free vibration given by:

$$w_n = A_n R_n (r) \cos (n\theta - \theta_g) \cos (p_n t - t_o)$$

This vibration is given with respect to the (r,θ) coordinate system fixed in the disk. For simplicity, let $\theta_0 = 0$, $t_0 = 0$ for the mode under consideration. Then:

(II.41) $$w_n = A_n R_n(r) \cos n\theta \cos p_n t$$

Using a trigonometric identity, equation (II.41) can be written as:

(II.42) $$w_n = \tfrac{1}{2} A_n R_n(r) \left[\cos (p_n t - n\theta) + \cos (p_n t + n\theta)\right]$$

Consider the first term of equation (II.42), which will be denoted as $w_n(1)$. That is:

$$w_n(1) = \tfrac{1}{2} A_n R_n(r) \cos (p_n t - n\theta)$$

This term, at any particular instant, is identical in form to the original mode shape given by equation (II.41). The same is true of the second term of equation (II.42). These two terms each contain "nodes", the locations of which, in general, are given by:

$$\theta(1) = \frac{p_n t}{n} \pm \frac{(2k + 1)\pi}{2n}$$

$$\theta(2) = \frac{-p_n t}{-n} \pm \frac{(2k + 1)\pi}{2n}$$

$$k = 0,1,2 \ldots$$

In addition, these "nodes" are moving in the disk at speeds of:

$$\dot{\theta}\,(1) = \frac{p_n}{n}$$

(II.43) $$\dot{\theta}\,(2) = \frac{-\,p_n}{n}$$

We conclude therefore that the response of equation (II.41) may be considered equivalently as consisting of two shapes, each identical to the shape of the mode itself, but of half the amplitude, and which are travelling in opposite directions around the disk.

The above results are stated with respect to the (r,θ) corodinate system. If the disk is rotating, the response with respect to the non-rotating coordinate system (r,γ) may be obtained with the use of the previously given transformation:

$$\theta = \Omega t - \gamma$$

To avoid confusion, the response as observed from the stationary coordinate system will be denoted u_n. Substitution of the transformation into equation (II.42) yields:

$$u_n = \tfrac{1}{2} A_n R_n (r) \left[\cos(p_n t + n\gamma - n\Omega t) + \cos(p_n t - n\gamma + n\Omega t)\right]$$

The response will be observed at some point in space, say $\gamma = 0$, in which case it can be written as:

(II.44) $$u_n = \tfrac{1}{2} A_n R_n (r) \left[\cos(p_n - n\Omega)t + \cos(p_n + n\Omega) t\right]$$

The frequencies seen by a space stationary observer, denoted by f_n, are therefore:

$$f_n = \begin{cases} p_n - n\Omega \\ p_n + n\Omega \end{cases} \tag{II.45}$$

Equations (II.45) are very useful since they yield a simple method of determining the particular mode shape associated with a resonance peak. The method is to excite the disk randomly and record the observed natural frequencies at several rotational speeds. The observed frequencies f_n as a function of the rotational speed Ω would appear as shown on figure 6 (neglecting imperfections). It can be seen that at low rotational speeds the slopes of the lines are approximately $\pm n$.

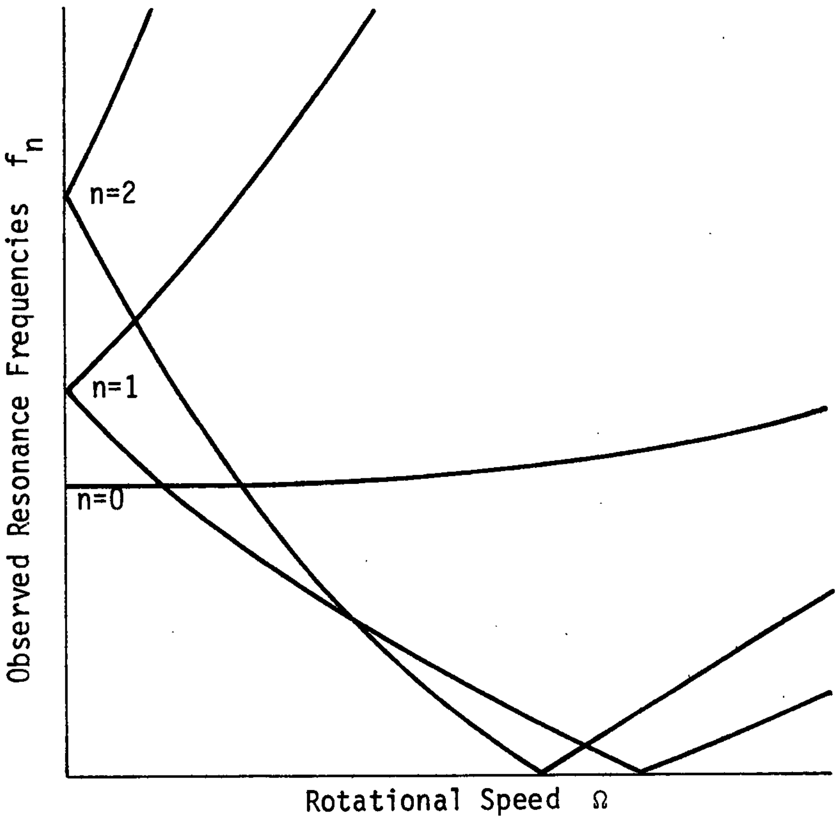

Figure 6

Observed Resonance Frequencies versus Rotational Speed

This result may be interperted physically by considering the two components of a mode as given by equation (II.42). When the disk is not rotating these two components, which are travelling in opposite directions at the same speed in the disk, are also travelling at equal but opposite speeds in space. However, when the disk is rotating, the component travelling in the direction of rotation, the "forward-travelling component", is moving faster in space than when the disk is stationary. Just the opposite is true of the "backward-travelling component".

A significant phenomenon may be noticed in figure 6. At some rotational speed one observed frequency of each mode, except for n = 0, becomes zero. From equation (II.45-a) for $f_n = 0$, we have:

$$p_n = n\Omega$$

If this value of P_n is substituted into the expression for the speed of the backward-travelling component, equation (II.43-a), the result is:

$$\dot{\theta}(1) = \Omega$$

Since the positive θ direction is that opposite to the rotation, it can be seen that the backward-travelling component is stationary in space. Similarily, the forward-travelling component is travelling at twice the disk speed. As the rotational speed is increased even further, the backward-travelling component actually begins to move forwards in space.

The above description does not consider the effects of either imperfections or rotational stresses. The existence of imperfections will double the number of observed frequencies, while the rotational stresses will increase their values in accordance with the relationship given by equation (II.40). The observed frequencies of the n nodal diameter vibration considering these two effects is then:

$$f_n = \begin{cases} \sqrt{p_{Bn}^2 + V_{n1}\Omega^2} \pm n\Omega \\ \\ \sqrt{q_{Bn}^2 + V_{n2}\Omega^2} \pm n\Omega \end{cases}$$

The lower branches of these observed frequencies become zero when:

$$\Omega^2 = \begin{cases} \dfrac{p_{Bn}^2}{n^2 - V_{n1}} \\ \\ \dfrac{q_{Bn}^2}{n^2 - V_{n2}} \end{cases}$$

Apparently when $V_n > n^2$ there is no possibility of the observed frequency becoming zero. Physically this occurs when as the rotational speed increases, the speed in the disk of the backward travelling component is increasing at a faster rate. This phenomenon does in fact occur in practice as will be shown experimentally in a later chapter.

If an observed frequency does become zero, the rotational speed at which this occurs is very significant when the forced response of rotating disks is considered. This is investigated in the following section.

II.6 Forced Response of a Disk[6]

The transverse loading of a circular saw arises from the interaction with the work piece. Since this transverse load is dependent on many factors, primarily the wood itself, its spectral density function is unknown. What is known, however, is that there is generally a significant load at a very low frequency, usually taken to be zero. The theory of a rotating disk responding to a static, space stationary point load is referred to as the "critical speed theory". This theory has been verified with circular saws in their working environment.[24]

The load used in the following development is taken to be P $\cos\omega t$, since a static load may then be taken as a specific case of a more general result.

The energy method is used here to determine the forced response of imperfect disks. When the effects of imperfections are neglected the response of a perfect disk is obtained. While it is possible to determine the forced response of a rotating disk and consider the non-rotating response as a special case, this is not the approach taken here. The non-rotating and rotating cases are treated separately, since one aspect of the problem, the damping, is significantly different.

Non-rotating Disk

For an imperfect disk, the free vibration in the n nodal diameter modes is taken to be:

$$w_{n1} = \Phi_n R_n \cos (n\theta - \alpha_n) \tag{II.46}$$

$$w_{n2} = \Psi_n R_n \sin (n\theta - \beta_n)$$

where Φ_n and Ψ_n are the normal coordinates previously denoted by ϕ_n and ψ_n.

The kinetic and strain energies of the non-rotating disk, from equations (II.32) are

$$\text{(II.47)} \qquad \begin{aligned} 2T_n &= A_n \dot{\Phi}_n^2 + B_n \dot{\Psi}_n^2 \\ 2U_n &= \bar{A}_n \Phi_n^2 + \bar{B}_n \Psi_n^2 \end{aligned}$$

The damping of this system is known to be very small. Experimental results, given in a later chapter, verify that the damping may be neglected when considering the forced response except when the disk is oscillated at very close to one of its natural frequencies. In order to provide a theoretical basis for this experimental result, damping will be assumed to be viscous, in which case the energy dissipated may be expressed as:

$$\text{(II.48)} \qquad 2D_n = G_{n1} \dot{\Phi}_n^2 + G_{n2} \dot{\Psi}_n^2$$

In using Lagrange's equation it is necessary to determine the generalized force associated with the load $P \cos\bar{\omega}t$. The generalized force is the quantity selected such that the product of this quantity and a virtual change in the generalized coordinate is equivalent to the virtual work done. Since each configuration from equation (II.46) behaves independently there will be two generalized forces associated with the n nodal diameter response.

The load P cos ωt is located at (r_p, θ_p). The displacement of the load due to a motion in the first configuration is:

$$w_{n1}(r_p, \theta_p) = \Phi_n R_n(r_p) \cos(n\theta_p - \alpha_n)$$

The work done δW_{n_1} during a virtual change in Φ_n is given by:

$$\delta W_{n_1} = P \cos \omega t \; R_n(r_p) \cos(n\theta_{pp} - \alpha_n)\, \delta\Phi_n$$

and similarily for δW^2_{n2}.

The generalized forces are therefore:

(II.49) $$M_1 = P R_n(r_p) \cos(n\theta_p - \alpha_n) \cos \omega t$$

$$M_2 = P R_n(r_p) \sin(n\theta_p - \beta_n) \cos \omega t$$

Lagrange's equations are:

$$\frac{d}{dt}\left(\frac{\partial T}{\partial \dot{\Phi}_n}\right) + \frac{\partial D}{\partial \dot{\Phi}_n} + \frac{\partial U}{\partial \Phi_n} = M_1$$

(II.50)

$$\frac{d}{dt}\left(\frac{\partial T}{\partial \dot{\Psi}_n}\right) + \frac{\partial D}{\partial \dot{\Psi}_n} + \frac{\partial U}{\partial \Psi_n} = M_2$$

which is the standard form for a viscously damped forced system. Solving for Φ_n and Ψ_n and substituting into equations (II.46) results in:

(II.51)
$$w_{n_1} = \frac{P\,R_n(r_p)\,R_n(r)\cos(n\theta_p - \alpha_n)\cos(n\theta - \alpha_n)\cos(\omega t - \eta_n)}{A_n\sqrt{(p_n^2 - \omega^2)^2 + \left(\frac{G_{n_1}}{A_n}\right)^2 \omega^2}}$$

$$w_{n_2} = \frac{P\,R_n(r_p)\,R_n(r)\sin(n\theta_p - \beta_n)\sin(n\theta - \beta_n)\cos(\omega t - \zeta_n)}{B_n\sqrt{(q_n^2 - \omega^2)^2 + \left(\frac{G_n}{B_n}\right)^2 \omega^2}}$$

where $p_n^2 = \bar{A}_n/A_n$; $q_n^2 = \bar{B}_n/B_n$

and $\eta_n = \tan^{-1}\dfrac{(G_{n_1}/A_n)}{(p_n^2 - \omega^2)}$

$\zeta_n = \tan^{-1}\dfrac{(G_{n_2}/B_n)}{(q_n^2 - \omega^2)}$

These equations are the most general form of the n nodal diameter response of a non-rotating imperfect disk to a point load of magnitude P cos ωt. In general there is a response in both configurations. If, however, the load is located at $\theta_p = \frac{1}{n}(\alpha_n + \frac{\pi}{2})$ or $\theta_p = \bar{\beta}_n/n$, there will be no response in configuration one or two, respectively. These are the locations of the free vibrations nodes of these configurations. Recalling that the nodes of one configuration are located approximately at the anti-nodes of the other ($\alpha_n \approx \bar{\beta}_n$), the maximum amplitude of the response of one configuration is obtained when the amplitude of the other is a minimum.

It is also apparent from equation (II.51) that if the excitation frequency is $p_n(q_n)$, the response will be almost entirely in configuration one (two), unless the load is applied at or near a node of that configuration.

Both of the above observations are useful experimentally when the validity of equations (II.51) is examined, and when the extent to which a disk is imperfect is to be determined.

One check of equations (II.51) that does not require a physical experiment is to observe the result when the disk is considered to be perfect. The vibration must be symmetric about the load irregardless of its location, with an anti-node located at the point of application of the load. If the disk is perfect $\alpha_n = \beta_n$, $A_n \doteq B_n$, $p_n = q_n$ and $G_{n1} = G_{n2}$. The n nodal diameter response may then be written as:

$$w_n = \frac{P\, R_n(r_p)\, R_n(r) \cos(\omega t - \eta_n)}{A_n \sqrt{(p_n^2 - \omega^2)^2 + \left(\frac{G_n}{A_n}\right)^2 \omega^2}} \Big[\cos(n\theta_p - \alpha_n) \cos(n\theta - \alpha_n)$$

$$+ \sin(n\theta_p - \alpha_n) \sin(n\theta - \alpha_n) \Big]$$

$$\doteq \frac{P\, R_n(r_p)\, R_n(r) \cos(\omega t - \eta_n)}{A_n \sqrt{(\bar{p}_n^2 - \omega^2)^2 + \left(\frac{G_n}{A_n}\right)^2 \omega^2}} \cos n(\theta_p - \theta)$$

As can be seen, the response is as expected. It is also interesting to note that the response of a perfect disk is essentially the same as that of an imperfect disk when the load is applied at the node of one of the configurations. There would, however, be a small difference due to changes in the values of A_n, p_n and G_n caused by the presence of imperfections, and also because α_n is only approximately equal to β_n for an imperfect disk.

Rotating Disk

To facilitate the description of the forced response of a rotating disk, several terms must be defined:

1. fixed vibration: This is the usual form of the free vibration of a disk, given, for example, by:

   $$w_n = A_n R_n \sin n\theta \cos at$$

   where a is the frequency. The nodes, located at $\theta = 0, \frac{\pi}{n}, \frac{2\pi}{n} \ldots$ are rotating with the disk. This vibration may be written as:

(II.52) $$w_n = \tfrac{1}{2} A_n R_n [\sin (n\theta - at) + \sin (n\theta + at)]$$

   where the forward and backward travelling components are apparent. In non-rotating coordinates, this appears as:

(II.53) $$u_n = \tfrac{1}{2} A_n R_n [\sin (n\Omega t - n\gamma - at) \pm \sin (n\Omega t - n\gamma + at)]$$

2. travelling waves: These waves, backward and forward travelling, are identical in form to the backward and forward travelling components described above. However, the two components of the fixed vibration are of equal amplitude, whereas a single wave may exist by itself. A backward travelling wave is given by:

(II.54) $$w_n = A_n R_n \sin (n\theta - at)$$

$$u_n = A_n R_n \sin (n\Omega t - n\gamma - at)$$

and a forward travelling wave by:

(II.55) $$w_n = A_n R_n \sin(n\theta + at)$$

$$u_n = A_n R_n \sin(n\Omega t - n\gamma + at)$$

3. steady deflection: If the rotational speed Ω and the frequency a are such that $n\Omega = a$, the backward travelling component or backward travelling wave becomes stationary in space. For example, substituting $a = n\Omega$ into equation (II.54) for u_n yields:

(II.56) $$u_n = -A_n R_n \sin n\gamma$$

This is not a function of time. If the steady deflection is a result of a backward travelling component becoming stationary in space, the forward travelling component will be travelling at twice the disk speed, yielding an observed frequency of $f_n = 2n\Omega$.

The method of determining the forced response of a rotating disk is very similar to that for a non-rotating disk. The kinetic energy of the transverse vibrations is the same in both cases. The potential energy U_n is of the same form, except the coefficients $\bar{A}_n$ and $\bar{B}_n$ are now functions of Ω due to the membrane stresses.

The damping is a particularily difficult problem since the vibration will suffer significant windage at high rotational speeds. Although viscous damping has been assumed in the past,[6,15] it is unjustified since, for example, the windage suffered by a backward travelling wave is significantly less than that of a forward travelling wave. As well as being a function of the transverse velocity, the damping will also be a function of the rotational speed and the instantaneous amplitude of the transverse displacement. Except at near resonance, the effect of damping is quantitative only; the nature of the response is the same as in the undamped case. In the absence of a reasonable theoretical means of including the effects of damping it will be neglected in the theory that follows.

The generalized forces may be determined in the same way as for a non-rotating disk except that the location θ_p of the load varies. It is assumed that $\alpha_n = \beta_n$ and this angle is taken to be zero in the disk coordinate system. Since both origins are coincident at $t = 0$ and the load is taken to be located at $\gamma = 0$, its disk coordinates are $(r_p, \Omega t)$. The generalized forces are then:

$$M_1 = P\, R_n\,(r_p) \cos n\Omega t \cos \omega t$$
$$M_2 = P\, R_n\,(r_p) \sin n\Omega t \cos \omega t$$

which may be written as:

$$M_1 = \tfrac{1}{2} P\, R_n\,(r_p)\,[\cos(\omega + n\Omega)t + \cos(\omega - n\Omega)t]$$
$$M_2 = \tfrac{1}{2} P\, R_n\,(r_p)\,[\sin(\omega + n\Omega)t - \sin(\omega - n\Omega)t]$$

Applying Lagrange's equations, the response is found to be:

(II.57)
$$w_{n_1} = \tfrac{1}{2} P\,[R_n(r_p)/A_n]\; R_n(r) \cos n\theta \left[\frac{\cos(\omega + n\Omega)t}{[p_n^2 - (\omega + n\Omega)^2]} + \frac{\cos(\omega - n\Omega)t}{[p_n^2 - (\omega - n\Omega)^2]} \right]$$

$$w_{n_2} = \tfrac{1}{2} P \left[R_n(r_p)/B_n \right] R_n(r) \sin n\theta \left[\frac{\sin(\omega + n\Omega)t}{[q_n^2 - (\omega + n\Omega)^2]} - \frac{\sin(\omega - n\Omega)t}{[q_n^2 - (\omega - n\Omega)^2]} \right]$$

The natural frequencies p_n and q_n here are functions of the rotational speed Ω, since they are obtained from the ratios:

$$p_n^2 = A_n / \bar{A}_n$$

$$q_n^2 = B_n / \bar{B}_n$$

The coefficients A_n and B_n are not functions of the rotational speed, so it can be seen from equations (II.57) that if the natural frequencies are known either from experimentation, or approximately from equation (II.40), that the only unknown effect of rotation is on the radial functions $R_n(r)$.

When $\Omega = 0$, equations (II.57) reduce to the previously developed expression for the response of a non-rotating disk subjected to a load $P \cos \bar{\omega} t$ located at an anti-node of configuration 1. The resonance condition is $p_n = \omega$.

However, when the disk is rotating there are four possible resonance conditions, given by:

$$\omega = p_n \pm n\Omega$$

$$\omega = q_n \pm n\Omega$$

These resonance frequencies coincide with what have previously been referred to as the observed natural frequencies of the disk. Although the response as predicted by equations (II.57) becomes infinite at any of these resonance frequencies because damping has been neglected, it can be seen that the response near resonance, when $\omega \approx p_n \pm n\Omega$ or $\omega \approx q_n \pm n\Omega$, is the shape and approximate frequency of the free response of the disk.

Since circular saw instability is known to be caused by a static load, the response to such a load will now be discussed in detail. Under the action of a constant load P, the response, as given by equation (II.57) is:

(II.58) $$w_{n_1} = P\,F_{n_1} \cos n\theta \cos n\Omega t$$

$$w_{n_2} = P\,F_{n_2} \sin n\theta \sin n\Omega t$$

where $$F_{n_1} = \frac{R_n(r_p)\,R_n(r)}{A_n\,[p_n^2 - (n\Omega)^2]}$$

and $$F_{n_2} = \frac{R_n(r_p)\,R_n(r)}{B_n\,[q_n^2 - (n\Omega)^2]}$$

Resonance occurs when $p_n = n\Omega$ or $q_n = n\Omega$. If a non-rotating disk is subjected to a static load, and the rotational speed is then increased, the first speed at which resonance occurs is known as the critical speed. In general, it can be seen that this type of resonance occurs at the same rotational speed at which the backward travelling component of a free vibration would be stationary in space; that is, when $f_n = 0$.

If the disk is perfect, $p_n = q_n$ and $A_n = B_n$. In this case the response is:

$$w_n = w_{n1} + w_{n2}$$

$$= P\ F_n\ [\cos n\theta \cos n\Omega t + \sin n\theta \sin n\Omega t]$$

$$= P\ F_n\ [\cos (n\theta - n\Omega t)]$$

This is the expression for a backward travelling wave (see equation II.54). Substituting $\theta = \Omega t - \gamma$, the response in space-stationary coordinates is:

(II.59) $$u_n = P\ F_n \cos n\gamma$$

This backward travelling wave, being fixed in space, is what has been defined as a steady deflection. It is travelling in the disk but its speed at any rotational speed is such that it appears fixed in space. Resonance occurs when the speed of this wave in the disk becomes equal to the wave speed of the backward travelling component of the free vibration in this mode. This is the usual condition for resonance; the system is forced to respond at the rate at which it does freely.

When the effects of imperfections are included, the response to a static load is somewhat more complicated. In this case, the total n nodal diameter response from equation (II.58) is:

(II.60) $$w_n = P\ (F_{n_1} - F_{n_2}) \cos n\theta \cos n\Omega t + P\ F_{n_2} \cos (n\theta - n\Omega t)$$

The first term here is a fixed vibration of frequency $n\Omega$ and the second term is a backward travelling wave stationary in space. The frequency of the fixed vibration is such that its backward travelling component is also stationary in space, thus contributing to the steady deflection. Equation (II.60) may therefore be written as:

$$w_n = \tfrac{1}{2} P\ (F_{n_1} - F_{n_2}) \cos (n\theta + n\Omega t)$$
$$+ \tfrac{1}{2} P\ (F_{n_1} + F_{n_2}) \cos (n\theta - n\Omega t)$$

To a space-stationary observer this appears as:

(II.61) $$u_n = \tfrac{1}{2} P(F_{n_1} - F_{n_2}) \cos (2n\Omega t - n\gamma)$$
$$+ \tfrac{1}{2} P(F_{n_1} + F_{n_2}) \cos n\gamma$$

The observed frequency of the forward travelling component is $2n\Omega$, as previously discussed.

If p_n is considered to be the lower of the two natural frequencies of the n nodal diameter configurations, when $n\Omega$ is less than p_n, which is the range of rotational speeds of interest here, equation (II.61) may be written as:

$$u_n = \tfrac{1}{2} P \left[1 - \frac{A_n}{B_n} \left(\frac{p_n^2 - (n\Omega)^2}{q_n^2 - (n\Omega)^2} \right) \right] F_{n_1} \cos (2n\Omega t - n\gamma)$$

$$+ \tfrac{1}{2} P \left[1 + \frac{A_n}{B_n} \left(\frac{p_n^2 - (n\Omega)^2}{q_n^2 - (n\Omega)^2} \right) \right] F_{n_1} \cos n\gamma$$

As can be seen, the amplitude of the forward travelling component relative to that of the steady deflection increases as the critical speed is approached. Although the amplitude of the forward travelling component never exceeds that of the steady vibration, this theory, which neglects damping, predicts that they are of very nearly the same amplitude close to the critical speed. Recalling that a vibration fixed in the disk is composed of forward and backward travelling components of equal amplitude, at close to the critical speed the response can be seen to consist almost entirely of a fixed vibration. This contrasts with the response of a perfect disk, where only a steady deflection is present.

It must be remembered, however, that a fixed vibration is moving in space at the disk rotational speed, whereas the steady deflection is stationary in space. It is expected therefore that, due to windage the amplitude of the fixed vibration relative to that of the steady deflection will be significantly less than that predicted by the above theory. This is confirmed in a later chapter which offers experimental verification of the theory which has been presented here.

II.7 Comments on the Theory and its Applications

The responses of non-rotating and rotating imperfect disks to a transverse point load, given by equations (II.51) and (II.57), were determined in order to predict the behaviour of a circular saw in its operating environment. Although such a model neglects many factors, the theoretical results obtained have been verified in sawing operations as being fairly accurate in predicting certain aspects of a saw's behaviour, most significantly the critical speed.[24] One of the major advantages of of this model is that those factors which are important in determining the saw's behaviour are easily identified. Several of the areas of current research on saw vibrations are based on concepts which were discussed in the rotating disk theory.

Current Research

One of the most common methods of reducing the transverse motions of circular saws is known as tensioning, having been used in some form for approximately 100 years. Tensioning is the process of altering the saw membrane stresses to increase the critical speed of the saw.

The membrane stresses for an initially stress free saw are due to rotation only. The maximum rotational speed of the saw must be less than that speed at which a static load causes resonance. When rotationally induced membrane stresses only are present, this may be approximated by:

$$\Omega^2_{cr} = \frac{p^2_{Bn}}{n^2 - V_n}$$

This speed is dependent on the coefficient V_n which is a measure of the influence of the rotational stresses. It can be seen that if this influence could be increased, the result would be a higher critical speed.

One method of tensioning involves plastically deforming the saw in compression in a narrow annulus, indicated by the dashed line in figure 7.

When the saw is not rotating, the radial stresses will be compressive throughout, while the hoop stresses will be compressive on the inner portion of the saw, and tensile on the outer portion as shown. These initial stresses are such that when the saw is rotating at its rated speed all membrane stresses are tensile, although not of the same value as when the saw is not tensioned. Since the magnitude of the radial stress is reduced by this process, those modes whose membrane potential energies of deformation are due primarily to the radial stress will have reduced natural frequencies. These modes are those consisting of a low number of nodal diameters. However, due to the increase in the tensile hoop stress in the outer portion of the saw, those modes consisting of a larger number of nodal diameters will have an increase in their natural frequencies. With the correct amount of tension it is possible to increase the natural frequency of that mode which determines the critical speed of the saw.

Figure 7

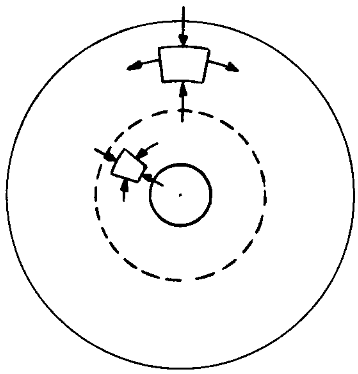

Membrane Stresses in a Non-rotating Tensioned Disk

The same result may be obtained by another method which is less common. If the saw is heated at the collar a thermal gradient will exist where the rim is at a lower temperature than the inner portion. This gradient may be selected such that the membrane stresses are similar to those described above, also resulting in an increase in the critical speed.

The effects of tensioning may be determined numerically for an idealized saw.[10,11] In practice, however, there are unknown factors which influence the optimum amount of induced tension, such as the heat generated by cutting. It is necessary that any method by which the desired amount of tension is determined be flexible to allow for the changing conditions of the operating environment.

A second major direction of research, altering saw geometries, has recently become of interest theoretically due to the availability of such techniques as the finite element method. One of the most common departures of saw geometries from those of perfect disks is the presence of holes and radial slots. Slots are particularly common for two reasons. Firstly, they inhibit the motion of waves travelling around the saw, and secondly, the compressive hoop stresses at the rim resulting from the heat generated during cutting are reduced because the saw can expand into the slots.

Although holes and slots cannot be considered small imperfections, they have the same effect as small imperfections on the amplitude of the steady deflection. It is possible, with the proper selection of holes and slots, to reduce the amplitude of this deflection. An approach currently being persued is the selection of the number, size and locations of holes and slots to optimize this amplitude reduction.[13,14]

As is the case with tensioning, the effects of holes and slots on the behaviour of an idealized saw can be determined numerically. Although this predicted response can be verified under controlled experimental conditions, verification in the field, which is the ultimate test, has in the past proven difficult to achieve.

Saw Behaviour in its Operating Environment

It is difficult to evaluate the performance of a circular saw in its operating environment by monitoring its transverse displacement. A more direct and simpler method is to observe the quality of the wood cut by the saw. This is in fact the method initially used to verify the critical speed theory.[24]

It may be desirable, however, to monitor the saw's displacement. This displacement may, for example, be used as an input for an automatic control scheme.[15,16] The difficulties encountered can be seen by considering the response predicted by the imperfect disk theory. As previously stated, the load is known to consist predominantly of a large static component, which results in a space-stationary backward travelling wave and a vibration fixed in the saw. In addition to this response, due to the very low damping of the system there is the possibility of an observable response at the natural frequencies due to random excitation. Considering these two types of responses, the observed frequencies as a function of rotational speed would appear as shown in figure 8. Here the responses in the $n = 1$ and $n = 2$ modes only are shown for clarity. Including the zero frequency responses, at any rotational speed the total response consists of responses at eleven different frequences. Since there will be responses in other modes as well, it can be seen that evaluating the behaviour of a saw at a particular rotational speed would be very difficult.

Figure 8

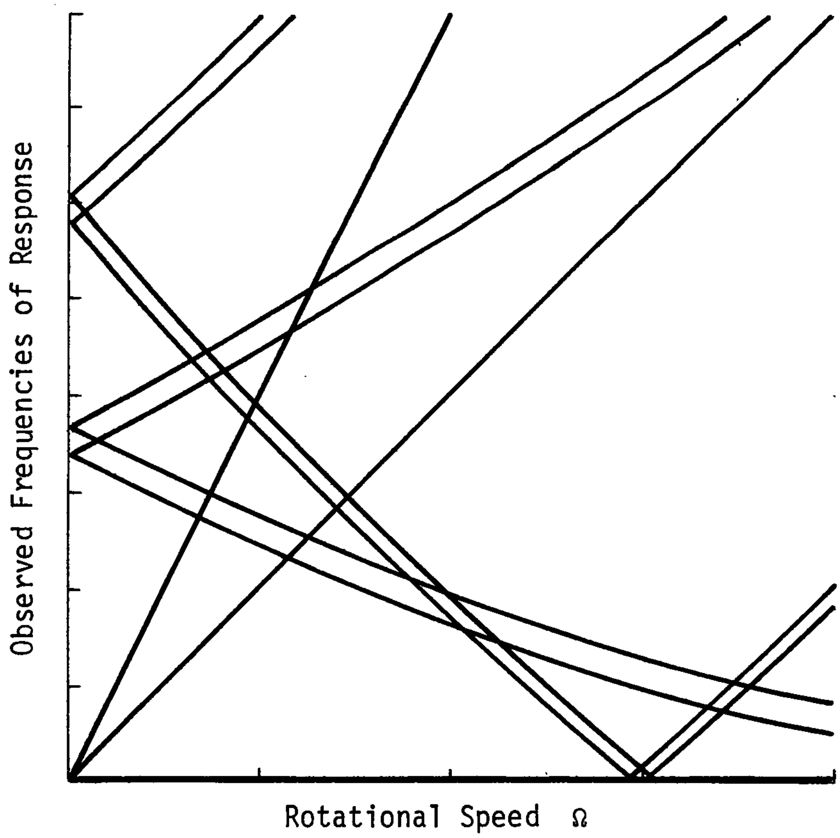

Saw Response versus Rotational Speed

Under laboratory conditions however, the situation is somewhat different. In this case the load can be carefully controlled and measured, and the rotational speed set at any desired level. It is then possible to investigate the validity of a theory under conditions more closely resembling those on which the theory was based. The next chapter describes experiments which were conducted to verify the theory which was developed in this chapter.

III Experimental Verification of the Theory of Rotating Disks

Experiments were devised to verify the theory presented in the previous chapter. The outcomes of this theory were the forced responses of non-rotating and rotating disks, given by equations (II.51) and (II.57). Before these results could be verified, it was necessary to conduct several preliminary experiments. For each result presented both the experimental and the theoretical means used to obtain the result are described in detail.

III.1 Experimental Equipment

The disks used to obtain the experimental results were prepared from steel blanks from which circular saws are manufactured. Their dimensions were:

	thickness	diameter
disk A	0.050"	18.4"
disk B	0.085"	18.2"
disk C	0.085"	18.2"
disk D	0.050"	18.3"

Although tests were conducted with all disks, only the results for disks C and D are given here since the other disks simply supported the results obtained with these two. All disks possessed no large imperfections and were complete except for a central hole approximately one inch in diameter. The collars used were three inches in diameter.

The collar assembly was press-fitted onto the rotor shaft of a one-half horsepower Reliance D.C. motor. The rotational speed was infinitely variable over a range of 0 to 2500 r.p.m., with the speed being monitored by a Dynamics Research Corp. incremental shaft encoder and displayed digitally.

The transverse motion of the disks was measured with space-stationary Bentley eddy current proximity sensors, and their accompanying power supply and drivers. Two sensors were calibrated, although most tests used only one. The calibration curve of this sensor is shown in figure 9. This curve was obtained with the use of a dial gauge.

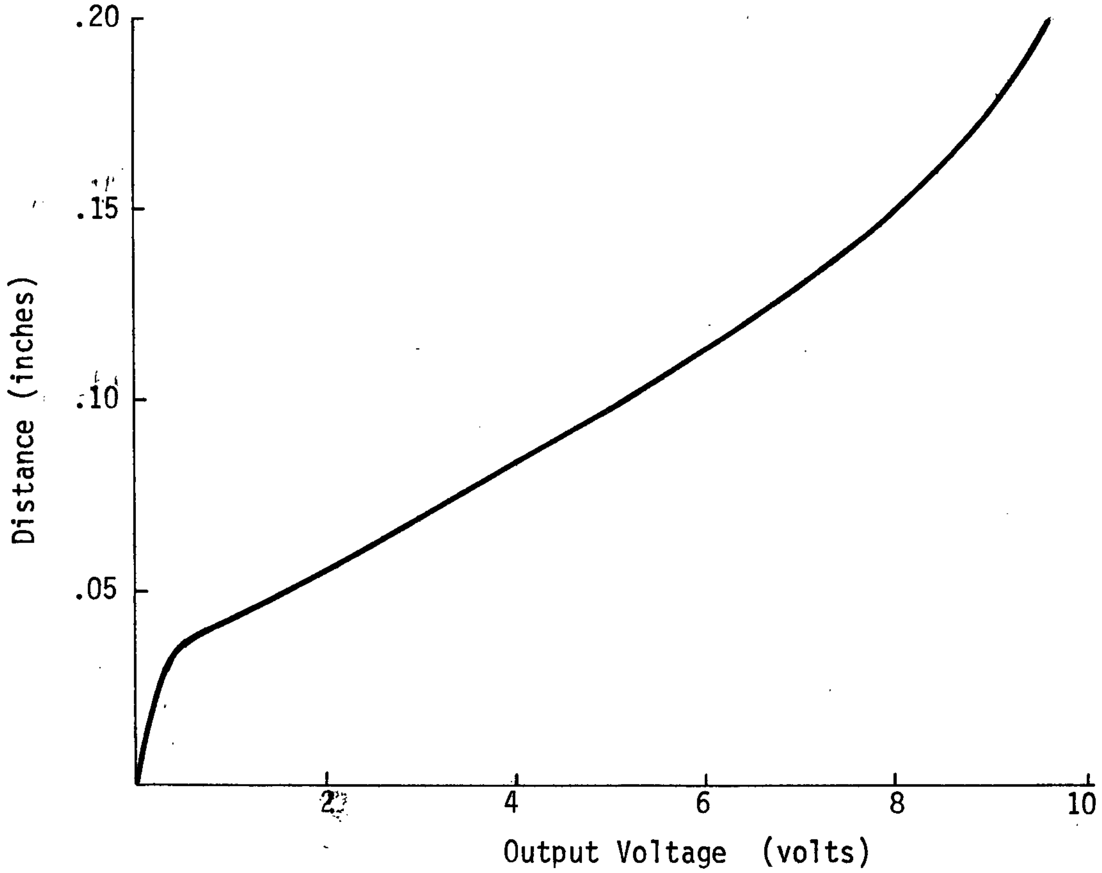

Figure 9
Proximity Sensor Calibration Curve

The proximity sensors were positioned approximately 0.10" from the surface of the disk, giving a linear response range of nearly ± 0.050". It was possible to position the sensors at any desired location in space.

A Spectral Dynamics Spectrascope II spectral analyzer was used to measure the response spectrum, and to ensure an accurate load frequency when the disk was excited sinusoidally. This is a single channel analyzer. It was used in close conjunction with a Telequipment model DM64 dual channel oscilloscope. The two channels of the oscilloscope allowed a direct observation of the phase differences between either the load and the response, or between the responses at two different points.

Disk excitation was provided by an electromagnet fixed in space at a distance of approximately one-quarter inch from the surface of the disk, at a radius of seven inches. Power to the electromagnet was supplied by a power amplifier, a D.C. power supply or both. The input to the power amplifier was an A.C. or random signal provided by a Bruel and Kjaer Type 1024 Sine-Random Generator.

The electromagnet was secured to a shaft which was inserted in a ball bushing allowing rotational and axial freedom. However, axial motion was prevented by securing the end of the electromagnet shaft to a Bruel and Kjaer Piezoelectric Force Transducer Type 8200, which was then connected to a heavy support. The output from this transducer was directed through a charge amplifier from which the magnitude of the force was continously available as a voltage. Calibration was obtained with the use of weights which were accurately weighed.

The free responses of the disks were not investigated experimentally because the presence of damping, even though very small, created difficulties in obtaining accurate measurements. All results given here are for the forced responses of the disks.

It was desirable to apply three types of loads to the disks; a static load, a sinusoidal load and a random load. The static load was achieved simply by applying a D.C. voltage to the electromagnet. A sinusoidal load, however, cannot be obtained with the use of only one electromagnet. When a load such as P $\cos\omega t$ was desired, this input was added to a D.C. voltage of magnitude P, yielding a resultant load of $P(1+\cos\omega t)$. Since the applied loads were of a magnitude such that the response was within the linear range, it was possible, in some cases, to obtain the response to a sinusoidal load by neglecting the D.C. component of the proximity sensor output. Applying a random load presents the same problem as does a sinusoidal load, but since a random load was used only for identifying resonance frequencies, this signal was not off-set by a D.C. voltage.

III.2 Forced Response of a Non-rotating Disk

The response of a non-rotating disk in its n nodal diameter modes to a load P $\cos\omega t$ is given by equation (II.51). The total response is:

$$w = \sum_n w_{n1} + w_{n2} \tag{III.1}$$

In this section it will be shown that the observed amplitudes and shapes of the response of a disk agree very closely with those determined theoretically.

The first step in obtaining this verification was to accurately determine the disk natural frequencies since the amplitude of the response is extremely sensitive to the differences between the excitation frequency and the natural frequencies. In order to determine the natural frequencies, the disk was excited randomly while it was not rotating and the resonance peaks displayed on the spectral analyzer were recorded. By rotating the disk slowly so that the influence of the rotational stresses was minimal, the values of n were determined by noting the rate of change of the observed frequencies with respect to the rotational speed, as previously discussed. The results are shown below for disk C.

Nodal Diameters	Disk Natural Frequencies (Hz)	
	Experimental	Theoretical
0	54.0	48.8
1	34.8, 35.2	40.1
2	61.4	62.2
3	125.0	124.7

The n = 1 configurations of this disk were the only two that displayed an observable difference in their natural frequencies. The knowledge of these two frequencies may be used to determine the location of the nodes of these configurations.

The Location of the Nodes

If the disk is excited at a frequency $\omega = p_1$, and the sensor is located at the point of application of the load, the responses in the n = 1 configurations are:

$$w_{11} = \frac{P\left[R_1(r_p)\right]^2 \cos^2(\theta_p - \alpha_1) \cos(\omega t - \eta_1)}{G_{11}\, p_1}$$

(III.2)

$$w_{12} = \frac{P\left[R_1(r_p)\right]^2_2 \sin^2(\theta_p - \beta_1) \cos(\bar{\omega} t - \zeta_1)}{\bar{B}_1 \sqrt{(q_1^2 - p_1^2)^2 + \left(\frac{G_{12}}{B_1}\right)^2 p_1^2}}$$

The response in these two configurations will be much larger than in any others, and the total response of the disk to this load may be approximated as $w = w_{11} + w_{12}$. In addition, it can be seen that, except when the load is applied at or near the node of configuration one, the response in this configuration will be much larger than in the other.

The natural frequencies, p_1 and q_1, of disk C were seen to be 34.8 and 35.2 Hz. The frequency of excitation was set initially at 34.8 Hz., and the load and proximity sensor were located at some arbitrary angle, with the amplitude of the response being noted. This was done at 15^0 intervals around the disk. The excitation frequency was then changed to 35.2 Hz. and the procedure was repeated. The results are shown in figure 10.

The origin of the coordinate system has been selected such that the anti-node of configuration two is located at $\theta = 0$. As expected, the node of configuration one is located approximately halfway between that of configuration two. In addition, the shapes of the two curves are very nearly $\cos^2(\theta-\alpha_n)$ and $\sin^2(\theta-\beta_n)$. The deviation from these shapes is due to several factors; the load covered a finite area rather than being a point load, there were responses in modes other than the one being resonated, and any change in the shape of the response due to imperfections was neglected theoretically.

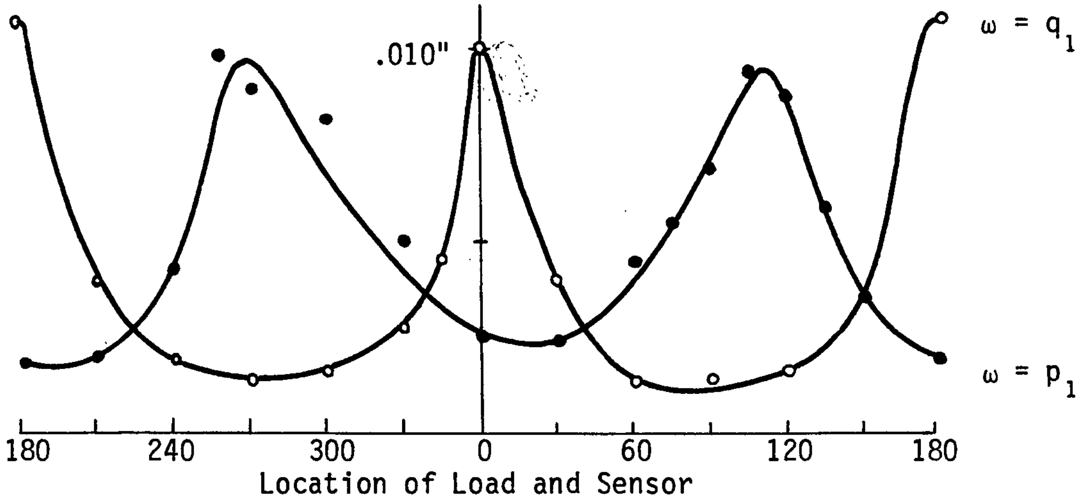

Figure 10

Amplitude of the Response versus Location of the Load

In addition to the location of the nodes, in order to calculate the theoretical response of the disk it is necessary to know the dissipation coefficients G_{n1} and G_{n2}. These could be determined approximately from equations (III.2) and the information presented in figure 10, but several practical problems arise. Most significantly, there is a dependence on the radial functions and these functions have yet to be verified. There is also a dependence on the magnitude of the load P, and its value at resonance must be so small to prevent a non-linear response that it cannot be accurately measured. Both of these problems are avoided by the method described below.

Damping Coefficient

If it is assumed that $\alpha_1 = \beta_1$, and if both the load and the sensor are located at a node of configuration two, the one nodal diameter response may be written as:

$$w_1 = \frac{P\,[R_1(r_p)]^2 \cos(\omega t - \eta_1)}{A_1 p_1 \sqrt{\left[1 - \left(\frac{\omega}{p_1}\right)^2\right]^2 + \left[\frac{2\xi\omega}{p_I}\right]^2}}$$

Here ξ is the damping factor; the ratio of the actual damping coefficient of the disk to its critical damping coefficient.[22]

The response will be predominantly in configuration one if the excitation frequency is close to p_I, and the load is applied at an antinode of this configuration. It is possible to non-dimensionalize this response and the excitation frequency. If the amplitude of the response is w_{1*} when $\omega = \omega_*$, the amplitude as a function of the excitation frequency can be written as:

$$\text{(III.3)} \qquad \left|\frac{w_1}{w_{1*}}\right| = \left\{ \frac{\left[1 - \left(\frac{\omega_*}{p_1}\right)^2\right]^2 + \left[2\,\xi\,\frac{\omega_*}{p_1}\right]^2}{\left[1 - \left(\frac{\omega}{p_1}\right)^2\right]^2 + \left[2\,\xi\,\frac{\omega}{p_1}\right]^2} \right\}^{1/2}$$

The experimental results are shown in figure 11 (dashed lines). For comparison purposes the theoretical results for $\xi = 0.00$, 0.01 and 0.02 are also plotted (solid lines).

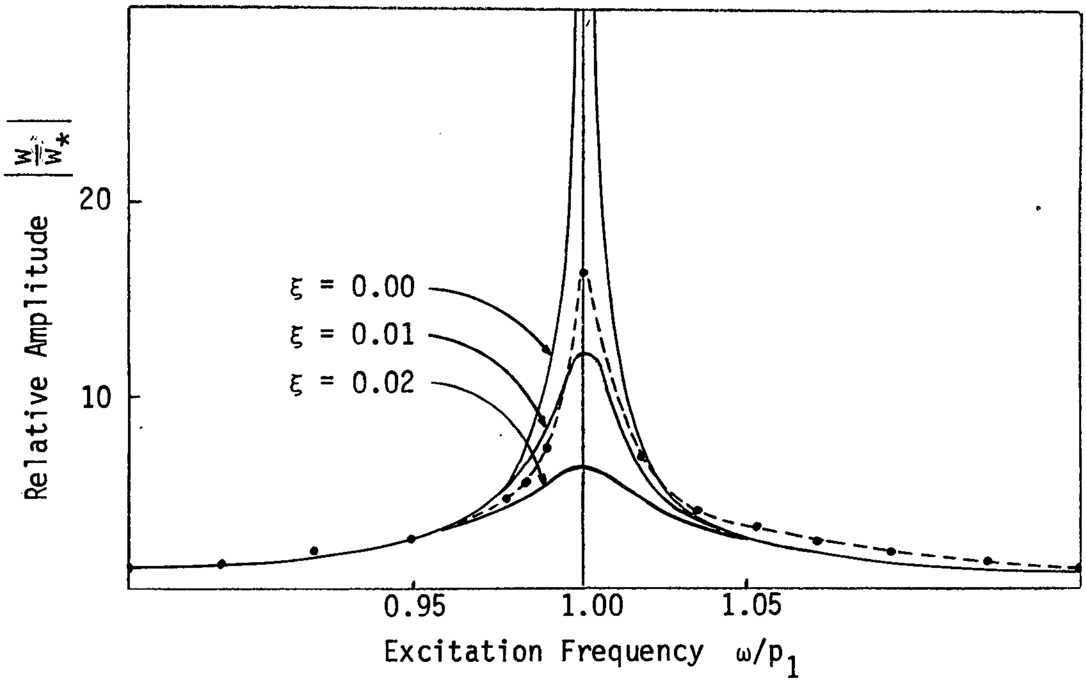

Figure 11
Relative Amplitude versus Excitation Frequency

It can be seen that the damping coefficient is less than 1% of critical. The response at frequencies above the resonance frequency is larger than expected due to responses in modes other than the one considered theoretically.

This experiment was also performed in the n = 2 mode. Here it was assumed that the disk was perfect since the natural frequencies p_2 and q_2 were indistinguishable. The damping coefficient was again found to be less than 1% of critical.

There are two effects of damping with which we are concerned. The first is its influence on the modal admittance. It can be shown that the difference in the admittance when calculated for $\xi = 0.00$ as compared to

$\xi = 0.01$ is less than 4% unless the excitation frequency is within 5% of the natural frequency.

The second effect of damping is the "smoothing out" of the phase change as the excitation frequency is varied from lower to higher than the natural frequency. The phase angle between the load and the response is:

$$\eta_n = \frac{2\xi\left(\frac{\omega}{p_n}\right)}{1 - \left(\frac{\omega}{p_n}\right)^2}$$

Unless the excitation frequency is within 5% of the natural frequency, the difference in phase for the two cases $\xi = 0.00$ and $\xi = 0.01$ is less than 11°.

Since neither an amplitude error of 4% nor a phase angle error of 11° are significant, the system damping may be neglected theoretically when the excitation frequency is not within 5% of a natural frequency of the disk.

When damping is neglected, it is possible to formulate approximate expressions for the radial and angular profiles of the disk using the radial functions obtained by the Rayleigh-Ritz method.

Radial and Angular Deflection Profiles

When a disk is excited by a load $\not{P}$ cos ωt, the total response is the sum of the responses of each mode. This requires that the location of the nodes of each configuration be known. It has been shown, however, that $\alpha_n = \beta_n$ approximately, and if the excitation frequency ω is such that any difference between p_n and q_n is negligible the theoretical imperfect disk response is equivalent to that of a perfect disk. This was the approach taken when the radial and angular profiles were determined for disk C. The excitation frequencies were 0 Hz and 90 Hz, which are suitable for neglecting both the differences in the natural frequencies of the configurations and the effects of damping.

In order to obtain a radial profile both the load and the sensor were located at $\theta = 0$. The sensor was positioned at various values of r where the amplitude of the response was noted.

The maximum amplitude of the deflection as a function of the radius is, from equation (II.51):

$$w(r) = \frac{R_0(r_p)\,R_0(r)}{A_0\,(p_0^2 - \omega^2)} + \frac{R_1(r_p)\,R_1(r)}{A_1\,(p_1^2 - \omega^2)} + \text{---}$$

For ω = 0 Hz, the predominant response was theoretically found to be in the n = 1 mode, whereas at ω = 90 Hz the n = 2 mode predominated. In both cases the contribution of the n = 4 mode was insignificant.

These profiles are shown in figures 12 and 13, where the solid lines are the theoretical profiles and the dashed lines are those measured.

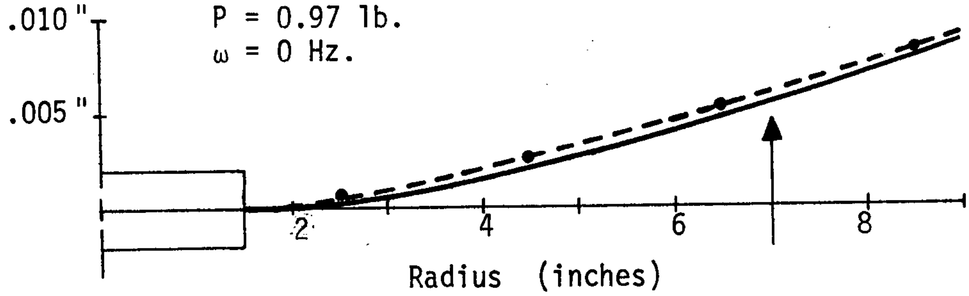

Figure 12

Radial Profile at 0 Hz. (Disk C)

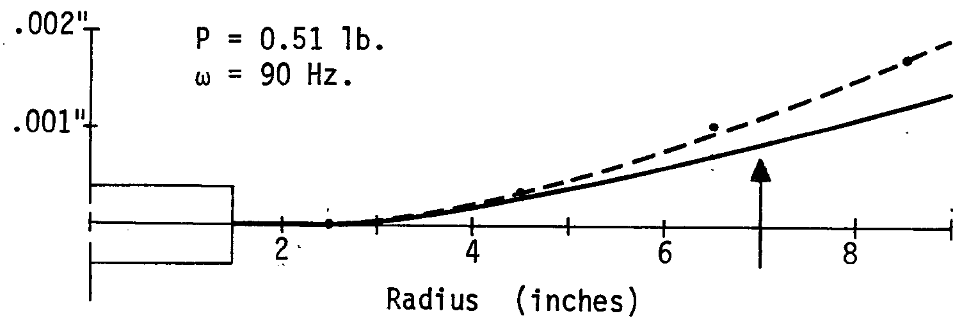

Figure 13

Radial Profile at 90 Hz. (Disk C)

It can be seen that although the load for the ω = 90 Hz case is approximately one half that of the ω = 0 Hz case, the response is reduced by roughly 80%. This is due to the much greater strain energy per unit deflection for the higher modes.

The angular profile was measured for a static load (0 Hz). The sensor was located at r = 8.5" and measurements were taken at 30^0 intervals around the disk. The theoretical angular profile is obtained from equation (II.51) which, neglecting damping is:

$$w(\theta) = \frac{PR_0\,(r_p)\,R_0\,(8.5)}{A_0\,(p_0^2 - \omega^2)} + \frac{PR_1\,(r_p)\,R_1(8.5)\cos\theta}{A_1\,(p_1^2 - \omega^2)} + \text{---}$$

To illustrate the relative magnitudes of the responses in the various modes, the theoretical responses for w_0 , w_1 , w_2 and w_3 are shown in figure 14. The predominance of the n = 1 mode can be observed.

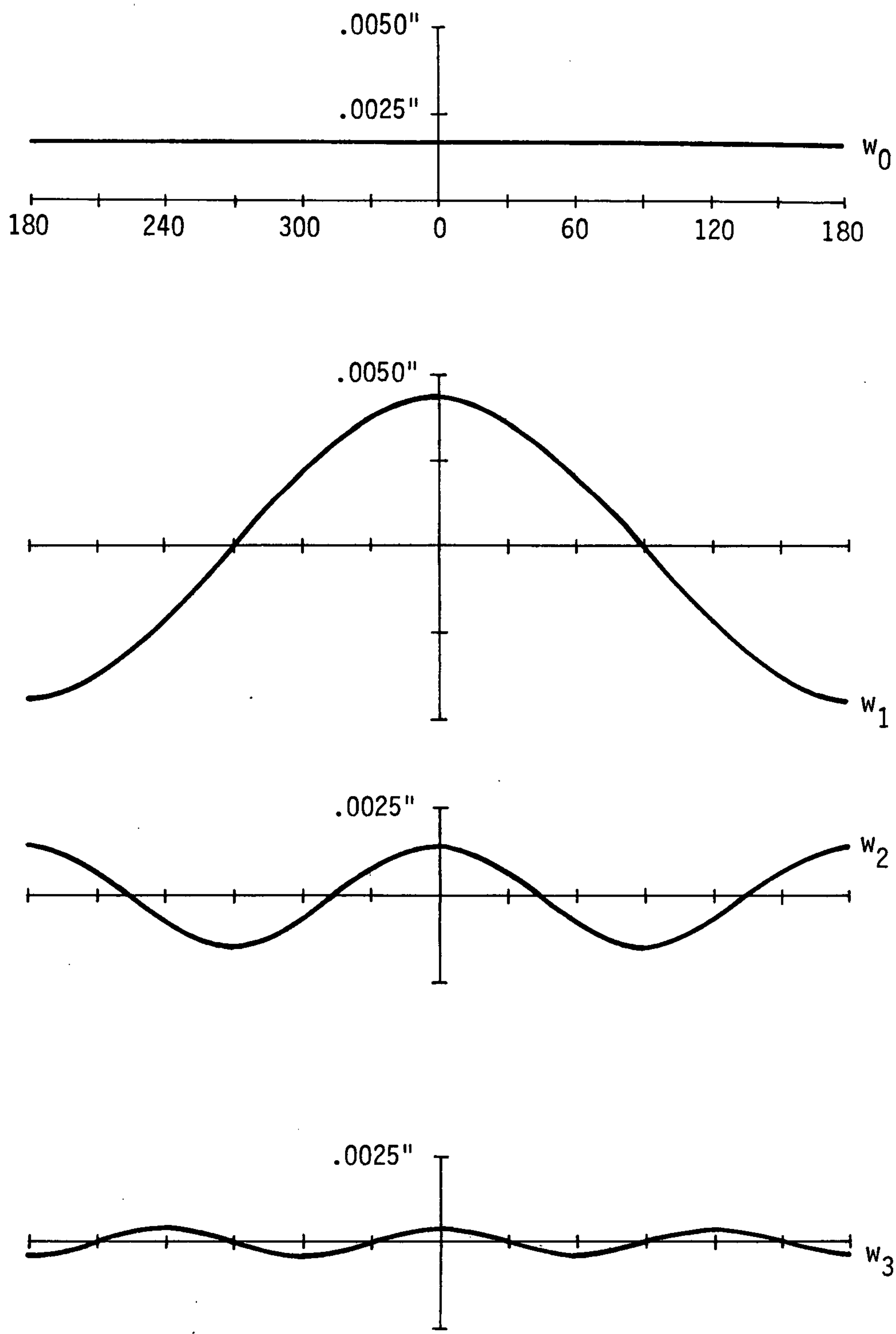

Figure 14

Theoretical Angular Profiles at 0 Hz.

The total theoretical profile w is plotted in figure 15 (solid lines) along with that measured (dashed line).

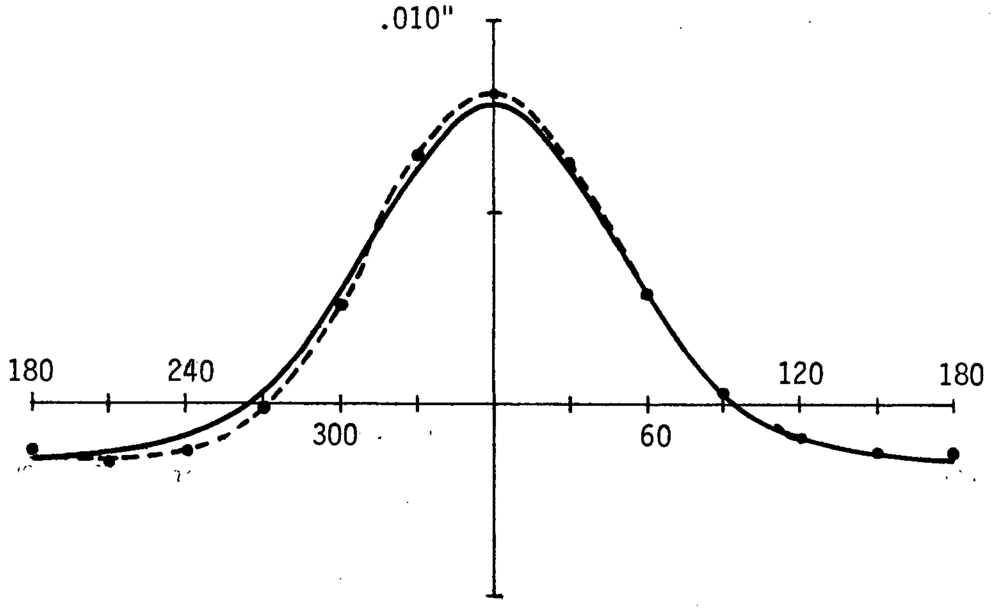

Figure 15

Angular Profile at 0 Hz. (Disk C)

Although the experimental results for one disk only have been presented here, these experiments were performed on the other disks as well, yielding results which also agreed very closely with the theoretical predictions.

III.3 Forced Response of a Rotating Disk

The n nodal diameter forced response of a rotating disk is given by equation (II.57). Because the response to a static load is of particular interest, it is this type of load for which the experimental results are presented. With this load the theoretical response is given by equation (II.58). As in the case of the non-rotating disk, it is essential to have accurate values of the disk natural frequencies, which are now a function of the rotational speed.

Observed Frequencies as a Function of Rotational Speed

There are two methods which may be used to determine the disk natural frequencies as a function of the rotational speed. The first method is by random excitation, as was done for the non-rotating disk. This is the method that was used to obtain the results presented here. The second method is somewhat more time consuming but is necessary under certain conditions. If, for example, the disk either contained slots, was not completely flat or was not running totally in a plane perpendicular to the shaft a significant response would be observed at integer multiples of the disk rotational speed. This would make the resonance peaks caused by random excitation difficult to identify. However, if at a particular rotational speed a sinusoidal load was applied and the frequency swept over the range of interest, from equation (II.57) it can be seen that a large response will occur when the excitation frequency corresponds to an observed natural frequency at that rotational speed.

By random excitation the graph of figure 16 was obtained for disk C. The difference between the natural frequencies of the two n = 1 configurations is clearly observable at all rotational speeds.

An approximate relationship for the natural frequencies was previously given as:

$$p_n^2 = p_{nB}^2 + V_n \Omega^2$$

For this disk, the values of V_1, V_2, and V_3 are 1.34, 2.91 and 5.90 respectively.[18] At 2500 r.p.m. this approximation yields frequencies which are significantly higher than those measured, being in error by 6.1%, 7.6% and 6.5% for the one, two and three nodal diameter modes. The size of these errors is attributable to the fact that for this disk and collar at 2500 r.p.m. the potential energy of the membrane stresses is not small in relation to that of the bending stresses, which is a requirement for an accurate approximation.

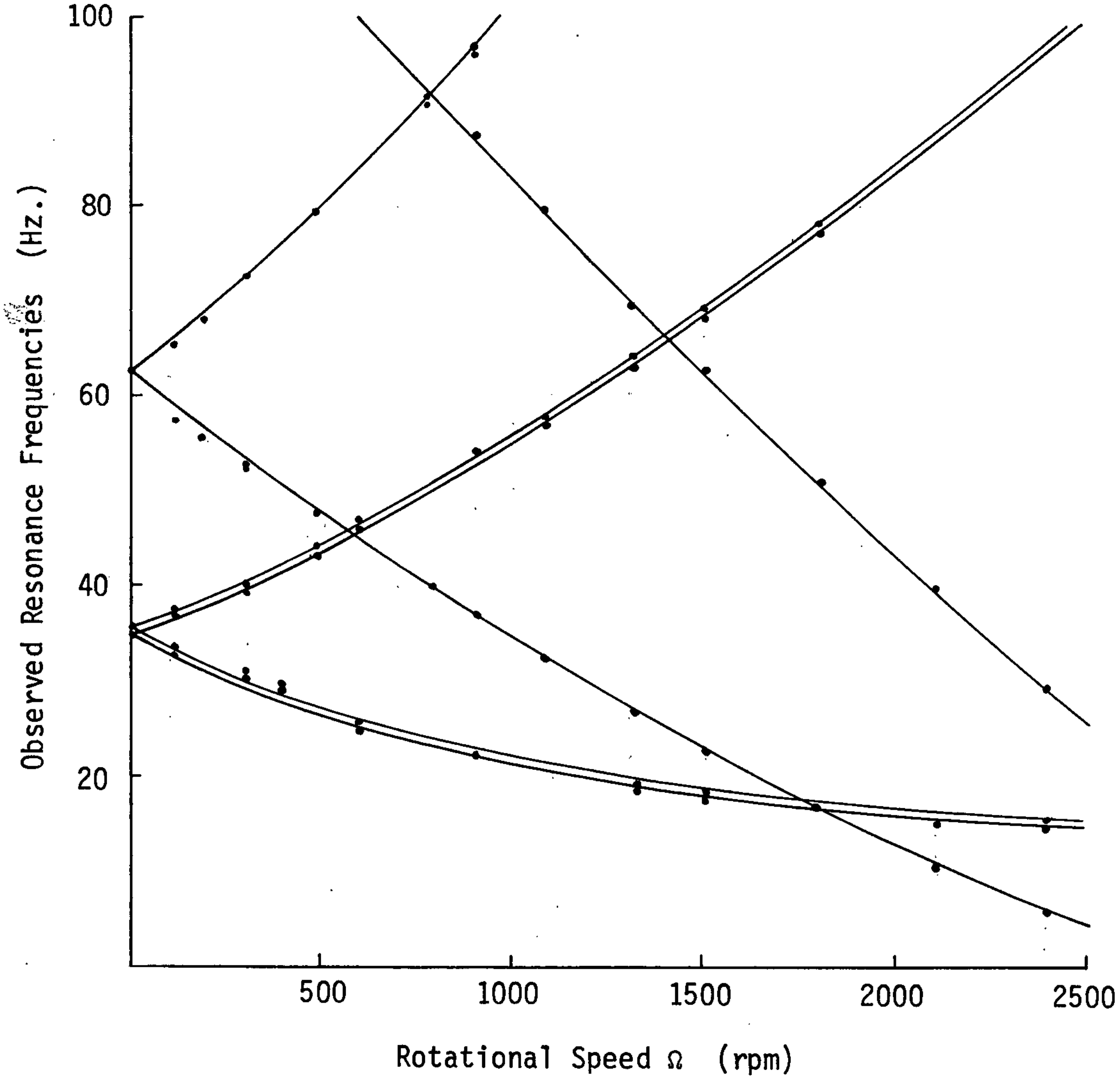

Figure 16

Observed Resonance Frequencies versus Rotational Speed

It was stated in Section II.4 that if $V_n > n^2$, there would be no possibility of an observed frequency of that mode becoming zero. In this case, $V_1 > 1$ and it can be seen from figure 16 that the lower branch of the observed frequencies of this mode will not intersect the horizontal axis. For this disk the critical speed is determined by the n = 2 mode, since it is this mode whose lower observed frequency first becomes zero.

Response to a Static Load

In the space-stationary coordinate system the n nodal diameter response to a static load located at $\gamma = 0$ is given by equation (II.61). For a perfect disk the total deflection at the load is:

$$u(\Omega) = \sum_n \frac{P\,[R_n\,(r_p)]^2}{A_n\,[p_n^2 - (n\Omega)^2]}$$

It is not immediately clear from this expression whether the rate of change of the amplitude with respect to the rotational speed is positive or negative at any particular speed. This is because the natural frequencies and to a lesser extent, the radial functions are dependent on the rotational speed.

This response was measured for disk C for rotational speeds varying from 0 to 2500 r.p.m. A theoretical response was calculated by assuming the radial functions were independent of the rotational speed, and by using the natural frequencies given in figure 16. The experimental results (dashed line) and theoretical results (solid line) are shown in figure 17.

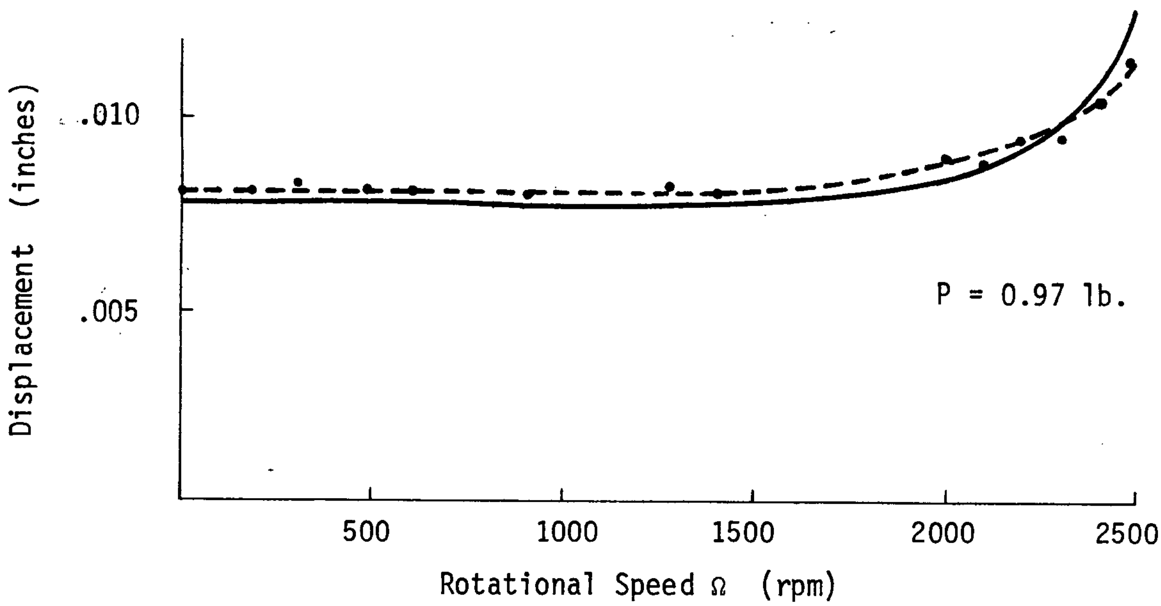

Figure 17

Displacement versus Rotational Speed (Disk C)

It can be seen that up to approximately 1500 r.p.m. the maximum deflection remains fairly constant. Although not shown on figure 17, this results from the fact that the deflections in the n = 0 and n = 1 modes are decreasing while those in the n = 2 and n = 3 modes are increasing.

The angular profile may also be determined from equation (II.61). For a perfect disk with the load located at $\gamma = 0$ and the sensor located at r = 8.5", it is given by:

$$u(\Omega,\gamma) = \sum_n \frac{P\, R_n\,(r_p)\, \bar{R}_n\,(8.5)\, \cos n\gamma}{A_n\,[p_n^2 - (n\Omega)^2]}$$

This profile was measured for disk C at 2400 r.p.m. and the results are shown in figure 18.

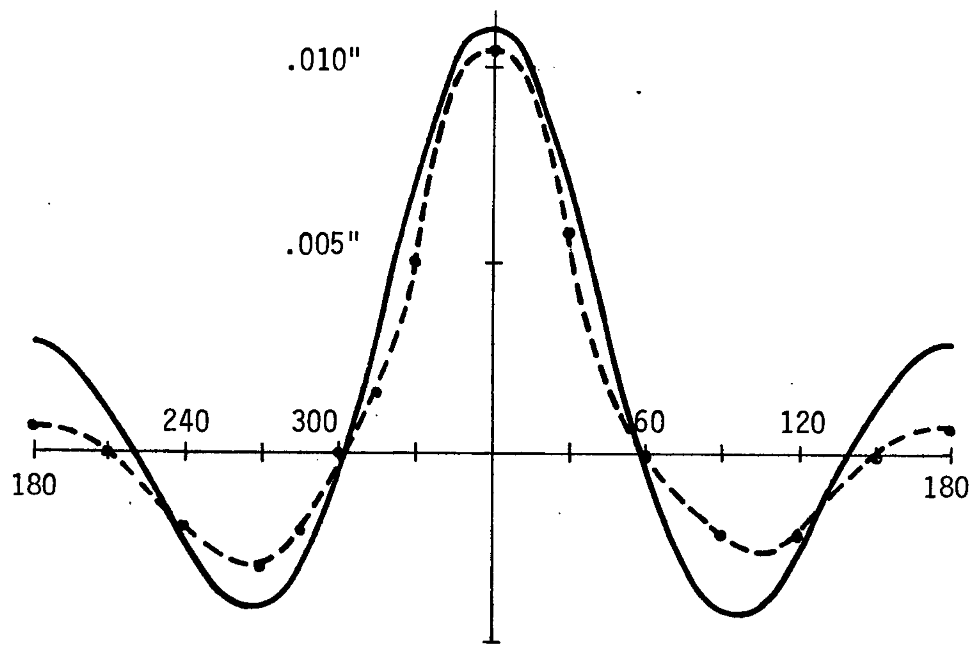

Figure 18

Angular Profile at 2400 RPM (Disk C)

The predominance of the n = 2 mode is observable. This profile may be compared with figure 15, which is for the same disk and load, except at zero rotation speed. In the non-rotating case, the "tilting mode", that is, the n = 1 mode, predominates.

The theoretical calculations done assumed that this disk was perfect. While this is not strictly true, at rotational speeds of less than 2500 r.p.m. the small differences between the natural frequencies of the configurations is inconsequential. One of the effects of imperfections is the existence of a $2n\Omega$ observed frequency. No such response could be detected for this disk at these rotational speeds.

These same experiments were conducted with disk D which is much thinner than disk C. The steady deflection as a function of the rotational speed is shown in figure 19, where the dashed line is the experimental result and the solid line is that determined theoretically.

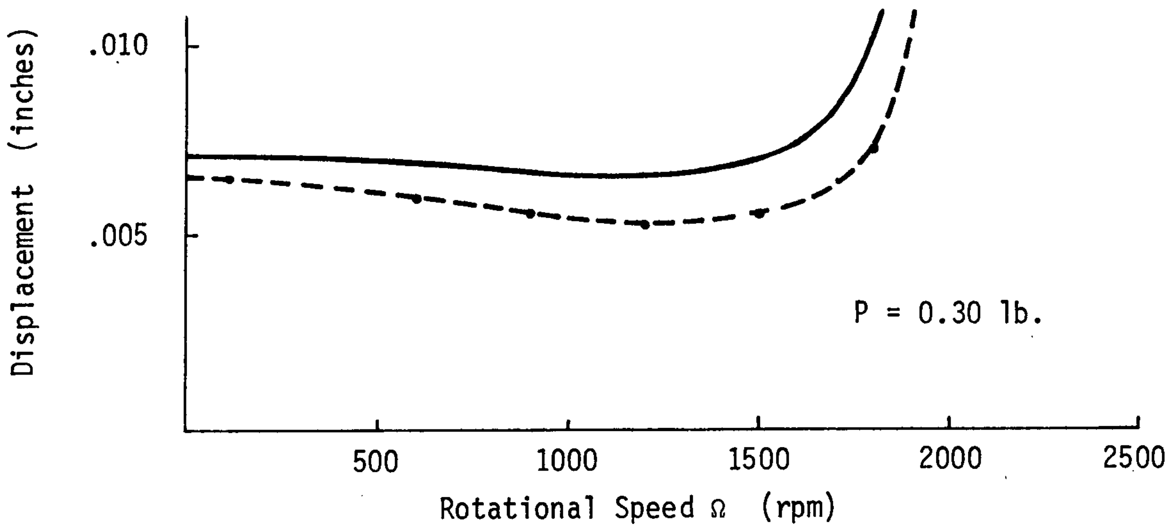

Figure 19
Displacement versus Rotational Speed (Disk D)

It can be seen that up to approximately 1200 r.p.m. the total deflection decreases with increasing rotational speed. Since this disk is quite thin (0.050"), the increase in the n = 0 and n = 1 natural frequencies due to an increase in the rotational stresses reduces the admittances of these modes to a greater extent than those of the n = 2 and n = 3 modes are increasing, resulting in a net decrease in the amplitude of the steady deflection. Above 1200 r.p.m. the response in the n = 2 mode begins to predominate, and near the critical speed of 2020 r.p.m., the angular profile is very similar to that shown in figure 18, since the critical speed of this disk is also due to resonance of the n = 2 mode.

The angular profile was measured at 1955 r.p.m. and the deflection under the load was found to be 0.014". However, at this speed a significant vibration at approximately 130 H_z was observed, with an amplitude of 0.0035". The frequency of this vibration is four times the disk rotational speed.

That this vibration is due to the forward travelling component of a fixed vibration is readily verified by the use of two proximity sensors, located at γ_A and γ_B in the space-fixed coordinate system. From equation (II.61) the forward travelling component as measured by each proximity sensor is given by:

$$u_{nA} = \tfrac{1}{2} P(F_{n_1} - F_{n_2}) \cos (2n\Omega t - n\gamma_A)$$

$$u_{nB} = \tfrac{1}{2} P(F_{n_1} - F_{n_2}) \cos (2n\Omega t - n\gamma_B)$$

These two signals may be observed simultaneously on a dual-beam oscilloscope, appearing as shown in figure 20.

Here the sensor B is assumed to be in the positive γ direction with respect to sensor A. Since the time t_d is $\frac{1}{2\Omega}[\gamma_B - \gamma_A]$, the phase difference between u_{nA} and u_{nB} expressed as a fraction of the wavelength is $\frac{n}{2\pi}[\gamma_B - \gamma_A]$.

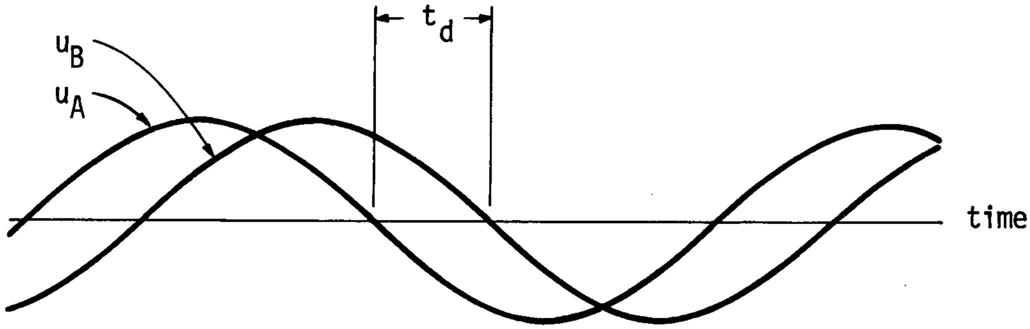

Figure 20

Forward Travelling Component Observed With Two Sensors

At 1955 r.p.m. the two natural frequencies p_2 and q_2 are 65.9 H_Z and 66.9 H_Z. The two nodal diameter response at this rotational speed may therefore be written as:

$$u_2 = \tfrac{1}{2}P\left[1 - 0.42\left(\frac{A_2}{B_2}\right)\right] F_{21} \cos\,(4\Omega t - 2\gamma)$$

$$+ \tfrac{1}{2}P\left[1 + 0.42\left(\frac{A_2}{B_2}\right)\right] F_{21} \cos 2\gamma$$

In order to evaluate this expression a knowledge of the nature of the imperfections is necessary so that the ratio A_2/B_2 can be determined. In general, the imperfections will effect both the kinetic energy ($A_n \neq B_n$) and the potential energy ($\bar{A}_n \neq \bar{B}_n$). However, by assuming first one type of imperfection and then the other, the amplitudes of neither the forward travelling component nor the steady deflection are significantly altered. For small imperfections, it may be assumed in this expression that $A_2 = B_2$.

It can be seen that due to the imperfections, the amplitude of the steady deflection is substantially decreased. At 1955 r.p.m. this decrease is roughly 25% that of the perfect disk steady deflection in the n = 2 mode. This aspect of the effect of the imperfections cannot be directly verified since the steady deflection due to a single mode cannot be accurately isolated from the total.

The amplitude of the forward travelling component, though, was measured (0.0035") and this compares quite well with the theoretical value of 0.005". It must be remembered that a vibration fixed in the disk is moving relative to the air, in this case in excess of 150 feet per second at the rim, and its amplitude is expected to be significantly less than that calculated neglecting windage.

Considering the assumptions made in order to obtain numerical values for the forced response of rotating disks the experimental results presented here are in fairly close agreement with the theoretical predictions. Although the quantitative agreement is not as good as in the non-rotating case, equation (II.57) has been shown to reasonably accurately represent the response of an imperfect rotating disk to a static load.

IV Closing Remarks

A theory has been presented here for the free and forced responses of non-rotating and rotating centrally clamped imperfect disks. Initially the free response of a non-rotating centrally clamped perfect disk was considered. In order to achieve a theoretical response which more closely agrees with experimental observations, the influence of small imperfections within the disk were then considered. The primary effects of these imperfections on the free response were shown to be that nodal lines exist at definite locations in the disk, and the natural frequencies of the two configurations of a nodal shape are different, the extent to which depends on the nature and magnitude of the imperfections.

To obtain a reasonable model of a circular saw it was necessary to consider the effects of rotational stresses on the disk's behaviour. It was shown that these effects can be determined by an approximation based on Southwell's Theorem. For disks of the physical dimensions and at rotational speeds typical of circular saws, this approximation yields acceptable results.

In determining the forced response of a disk, the load was taken as a transverse point load stationary in space. The forced responses of non-rotating and rotating imperfect disks were determined separately, and the perfect disk responses in both cases were achieved by simplifying a more general result. The primary use of the theoretical non-rotating disk response was for interpreting experimental results to determine the extent to which the disks were imperfect.

The rotating disk response to a transverse load was investigated in detail. For a perfect disk at any rotational speed, resonance of a mode consisting of nodal diameters was shown to be possible at two excitation frequencies. For an imperfect disk the response was similar except there were four resonance frequencies due to the frequency difference of the two configurations of each shape.

Of particular interest was the response to a static load since this is the basis of the circular saw critical speed theory. At rotational speeds well away from the resonance speed, the responses of perfect and imperfect disks were shown to be similar. However, as the resonance speed was approached these responses became very different. The perfect disk modal response to a static load was shown to consist entirely of a backward travelling wave stationary in space, whereas the imperfect disk response consisted of this wave plus a vibration fixed in the disk. The frequency of this fixed vibration was such that its backward travelling component was also stationary in space thus contributing to the steady deflection. The magnitude of the fixed vibration relative to that of the backward travelling wave increased as the resonance speed was approached. Near the resonance speed, this theory, which neglected damping, indicated that the response consisted almost entirely of a fixed vibration, contrasting significantly with the perfect disk resonance response.

The major aspects of the theory presented were verified experimentally. The agreement between theoretical and experimental results was good considering the theoretical approximations and experimental accuracy.

REFERENCES

1. Kirchoff, G.,"Ueber die Schwingungen einer elastischen Scheibe", Crelle's Journal, vol. 40, 1850.
2. Rayleigh, J.W.S., The Theory of Sound, New York, Dover Publications, 1945
3. Zenneck, J., "Ueber die freien Schwingungen nur annahernd volkommener kreisformiger Platten", 1899 Annalen der Physik, vol. 67, p.164.
4. Lamb, H. and Southwell, R.V., "The Vibrations of a Spinning Disk", Proc. Royal Soc. of London, vol.99, 1921, p. 272.
5. Southwell, R.V., "On the Free Transverse Vibrations of a Uniform Circular Disk Clamped at its Center; and on the Effects of Rotation," Proc. Royal Soc. of London, vol. 101, 1922, p. 133.
6. Tobias, S. A. and Arnold, R. N., "The Influence of Dynamical Imperfection on the Vibration of Rotating Disks", Inst. Mech. Engr. Proc., vol. 171, 1957, p. 669
7. Mote, C. D., "Effect of In-plane Stresses on the Vibration Characteristics of Clamped-free Discs", PhD Thesis, Department of Mechanical Engineering, University of California, Berkeley, 1963.
8. Dugdale, D. S., "Theory of Circular Saw Tensioning", The International Journal of Production Research, vol. 4, No. 3, 1966, p. 237.
9. Szymani, R., "Evaluation of Tensioning Stresses in Circular Saws", University of California Forest Products Laboratory, 1973.
10. Mote, C. D. and Nieh, L. T., "Control of Circular-disk Stability with Membrane Stresses", Experimental Mechanics, vol. 11, No. 11, p. 490, 1971

11. Mote, C. D., "Free Vibration of Initially Stressed Circular Disks" Trans. ASME, vol. 87B, p. 258, 1965

12. Nieh, L. T., "Rotating Disk Stability, Spectral Analysis and Thermal Effects", PhD Thesis, Department of Mechanical Engineering, University of California, Berkeley, 1972.

13. Dugdale, D. S., "Effect of Holes and Slots on Vibration of Circular Saws," Department of Mechanical Engineering, University of Sheffield, England.

14. Mote, C. D., "Stability Control Analysis of Rotating Plates by Finite Element: Emphasis on Slots and Holes", Trans. ASME, vol. 94G, p. 64, 1972

15. Ellis, W. E., "Active Electromagnetic Vibration Control in Rotating Discs", PhD Thesis, Department of Mechanical Engineering, University of California, Berkeley, 1976.

16. Radcliffe, C. J. and Mote, C. D., "On Line Control of Saw Vibration: Active Guides", Department of Mechanical Engineering, University of California, Berkeley, 1979.

17. Vogel, S. M. and Skinner, D. W., "Natural Frequencies of Transversely Vibrating Uniform Annular Plates", Trans. ASME, p. 926, December, 1965.

18. Eversman, W., "Transverse Vibrations of a Clamped Spinning Membrane", AIAA Journal, vol. 6, No. 7, p. 1395, 1968

19. Eversman, W. and Dodson, R.O., "Free Vibration of a Centrally Clamped Spinning Circular Disk", AIAA Journal, vol. 7, No. 10, p. 2010, 1969

20. Benson, R.C. and Bogy, D.B., "Deflection of a Very Flexible Spinning Disk Due to a Stationary Transverse Load", Trans ASME, vol. 45, p. 636, 1978

21. Timoshenko, S. and Woinowsky-Krieger, S., Theory of Plates and Shells, New York, McGraw-Hill, 1959

22. Thomson, W. T., "Vibration Theory and Applications", Englewood Cliffs, N. J., Prentice-Hall, Inc., 1965

23. Ritger, P. and Rose, N., "Differential Equations with Applications," New York, McGraw-Hill Book Company, 1968

24. Mote, C. D., "Verification of Saw Stability Theories", Department of Mechanical Engineering, University of California, Berkeley.